BBA - Molecular Basis of Disease 1870 (2024) 167198

Contents lists available at ScienceDirect

BBA - Molecular Basis of Disease

journal homepage: www.elsevier.com/locate/bbadis

A mouse model of autoimmune inner ear disease without endolymphatic hydrops

Shotaro Harada [a,b,1], Yoshihisa Koyama [a,c,d,e,*,1], Takao Imai [b], Yoshichika Yoshioka [f,g,h], Takuya Sumi [i], Hidenori Inohara [b], Shoichi Shimada [a,c,d]

[a] Department of Neuroscience and Cell Biology, Osaka University Graduate School of Medicine, Osaka 565-0871, Japan
[b] Department of Otorhinolaryngology-Head and Neck Surgery, Osaka University Graduate School of Medicine, Suita, Osaka 565-0871, Japan
[c] Addiction Research Unit, Osaka Psychiatric Research Center, Osaka Psychiatric Medical Center, Osaka 541-8567, Japan
[d] Global Center for Medical Engineering and Informatics, Osaka University, Suita 565-0871, Japan
[e] Integrated Frontier Research for Medical Science Division, Institute for Open and Transdisciplinary Research Initiatives (OTRI), Osaka University, Suita 565-0871, Japan
[f] Graduate School of Frontier Biosciences, Osaka University, Osaka 565-0871, Japan
[g] Center for Information and Neural Networks, National Institute of Information and Communications Technology (NICT) and Osaka University, Osaka 565-0871, Japan
[h] Institute for Open and Transdisciplinary Research Initiatives, Osaka University, Osaka 565-0871, Japan
[i] Department of Cell Biology, Graduate School of Medicine, Osaka University, Osaka 565-0871, Japan

ARTICLE INFO

Keywords:
Vertigo
Autoimmune inner ear disease
Type II collagen
Hearing loss
Rheumatoid arthritis

ABSTRACT

Autoimmune inner ear disease (AIED) is an organ-specific disease characterized by irreversible, prolonged, and progressive hearing and equilibrium dysfunctions. The primary symptoms of AIED include asymmetric sensorineural hearing loss accompanied by vertigo, aural fullness, and tinnitus. AIED is divided into primary and secondary types. Research has been conducted using animal models of rheumatoid arthritis (RA), a cause of secondary AIED. However, current models are insufficient to accurately analyze vestibular function, and the mechanism underlying the onset of AIED has not yet been fully elucidated. Elucidation of the mechanism of AIED onset is urgently needed to develop effective treatments. In the present study, we analyzed the pathogenesis of vertigo in autoimmune diseases using a mouse model of type II collagen-induced RA. Auditory brain stem response analysis demonstrated that the RA mouse models exhibited hearing loss, which is the primary symptom of AIED. In addition, our vestibulo-oculomotor reflex analysis, which is an excellent vestibular function test, accurately captured vertigo symptoms in the RA mouse models. Moreover, our results revealed that the cause of hearing loss and vestibular dysfunction was not endolymphatic hydrops, but rather structural destruction of the organ of Corti and the lateral semicircular canal ampulla due to an autoimmune reaction against type II collagen. Overall, we were able to establish a mouse model of AIED without endolymphatic hydrops. Our findings will help elucidate the mechanisms of hearing loss and vertigo associated with AIED and facilitate the development of new therapeutic methods.

1. Introduction

In 1979, Mac Bae reported that a type of cryptogenic, rapidly progressive sensorineural hearing loss, termed as “autoimmune sensorineural hearing loss,” could be successfully treated with immunosuppressive agents [1]. Later, the same condition was classified as autoimmune inner ear disease (AIED) after reports that it was often accompanied by vertigo [1]. The primary symptoms of AIED are progressive, fluctuating, and asymmetric sensorineural hearing loss with tinnitus, ear closure (25–50 %), and vertigo (50 %) [2]. AIED is divided into primary and secondary AIED, of which the latter includes diseases such as Cogan syndrome, Bechet's disease, relapsing polychondritis, systemic lupus erythematosus, rheumatoid arthritis (RA), inflammatory bowel disease, polyarteritis nodosum, and fibromyalgia [3]. One of

* Corresponding author at: Department of Neuroscience and Cell Biology, Osaka University Graduate School of Medicine, 2-2 Yamadaoka, Suita, Osaka 565-0871, Japan.
E-mail address: koyama@anat2.med.osaka-u.ac.jp (Y. Koyama).
[1] Equally contributed.

https://doi.org/10.1016/j.bbadis.2024.167198
Received 14 July 2023; Received in revised form 25 March 2024; Accepted 17 April 2024
Available online 25 April 2024

these diseases, RA, is thought to develop following the induction of autologous tissue destruction due to the following two causes: activation of macrophages caused by the activation of autoreactive effector helper T cells in response to self-antigens, and the action of autoantibodies produced by B cells directed by peripheral helper T cells. Although the exact autoantigen is unknown, type II collagen has been suggested as a candidate [4].

Type II collagen is composed of three polypeptide chains that form fibers and is abundantly localized in the cartilage tissue of the whole body, the vitreous body of the eye, and the inner ear [5]. Several rodent models in which arthritis is induced by immune sensitization to type II collagen have been developed [6,7], and have been reported to display inner ear disorders. Yoo et al. revealed that guinea pigs with RA induced by type II collagen dysfunction showed inner ear disorders such as degeneration of the stria vascularis, spiral ganglion cells, organ of Corti atrophy, and endolymphatic hydrops [8]. Auditory function has long been evaluated in detail using auditory brain stem response (ABR) analysis in experimental animals; however, vestibular function is difficult to evaluate in detail, and the pathogenic mechanisms underlying vertigo symptoms induced by autoimmunity are poorly understood. In our lab, we use a vestibular function test can accurately assess the vestibulo-oculomotor reflex (VOR), thus capturing a wide range of mild-to-severe vestibular functions [9].

In this study, we attempted to elucidate the pathophysiology and mechanism of hearing loss and vertigo symptoms associated with autoimmune diseases using a type II collagen-sensitized RA mouse model.

2. Materials and methods

2.1. Animals and model preparation

All experiments were performed using male 7-week-old DBA/1J mice (22–27 g; Japan SLC, Shizuoka, Japan). Mice were fed a standard diet (AIN93M; Oriental Yeast Co., Ltd., Tokyo, Japan) and water ad libitum and were maintained at a constant temperature (23–25 °C). Two groups of seven animals each were recruited for each experiment. One group was immunized with bovine type II collagen antigen (RA model group), while the other group was not immunized with bovine type II collagen antigen (normal group). The RA model was prepared as follows: equal amounts of the antigen solution (0.01 M acetate phosphate buffer containing 8 mg/mL bovine type II collagen) and the adjuvant solution (mixed solution containing dead *Mycobacterium tuberculosis* H37Ra and 4 mg/mL Freund's incomplete adjuvant) were placed in separate luer lock glass syringes, after which the antigen solution was transferred to the adjuvant solution. Subsequently, the syringes were alternately pushed and stirred to form emulsions. The prepared collagen solution was administered intradermally twice under isoflurane inhalation anesthesia. The first sensitization was administered intradermally at the base of the auricle at 8 weeks of age and the second sensitization was administered intradermally at the base of the tail three weeks after the first administration. The dosage was 0.025 mL/animal (0.2 mg/animal as a total amount of collagen) both times. Behavioral and morphological analyses were performed eight weeks after the second sensitization (Fig. 1A).

Model mice were evaluated using the following arthritis index on a 4-point scale (0, no change; 1, swelling of the toes; 2, swelling of the toes and soles; 3, swelling of the entire foot; and 4, severe swelling). If bone degeneration was observed, 1 point was added. A score of $\geq$1 was considered indicative of arthritis [10]. The hind limb edema rate was calculated using the following formula:

$$\text{Hindlimb edema rate}\ (\%) = (\text{Hindlimb volume after treatment} - \text{Hindlimb volume before treatment}) / \text{Hindlimb volume before treatment} \times 100$$

2.2. Behavior tests

Spontaneous activity and open field tests were performed to evaluate the RA mouse models. Rotarod, balance beam, and foot stamp tests were conducted to estimate vestibular function. Furthermore, a grip strength test was conducted to examine whether the outcome of vestibular function evaluation was caused by muscle weakness.

2.2.1. Measurement of spontaneous activity using Supermax system

Spontaneous activity was monitored individually in a home cage using a Supermex photocell beam system (Muromachi Kikai Co., Tokyo, Japan), as previously described [11]. The system was equipped with paired infrared pyroelectric detectors mounted at the center of the ceiling of the chamber as sensors. The sensor detects the radiated body heat of each mouse. The total spontaneous activity of mice was measured over 10 min, digitally converted, and saved. Data were analyzed using data accumulation software (CompACT AMS Ver.3; Muromachi Kikai Co.).

2.2.2. Open Field test

The experimental preparation was performed as previously described [11]. An open-field apparatus (Muromachi Kikai Co.) was used to assess spontaneous activity in a novel environment consisting of a square arena (500 mm × 500 mm) surrounded by a 400mm^3 wall. The open field test was initiated by placing the mouse in the center of the apparatus. Tracing of Mouse movements and recording of the total travel distance, average speed, and activity or inactivity time during the tests (10 min) were performed using video tracking system software (ANY maze; Muromachi Kikai Co.).

2.2.3. Rotarod test

Fore and hind limb motor coordination and balance were estimated using an accelerating rotarod device (MK-610 A; Muromachi Kikai Co.), as previously described [11]. The mice were placed on a rod (3 cm in diameter) with constant low-speed rotation (4 rotations per a minute: rpm, 30 s) to habituate them to walking. The rotation test was initiated at 4 rpm, and was gradually accelerated to 30 rpm over 5 min. The duration of the stay on the rod was automatically measured. Two trials were conducted for each mouse in a single test set. Statistical comparisons between the groups were performed using the average of two trials.

2.2.4. Balance beam test

Motor coordination and balance were evaluated using a custom-made balance beam set, based on previous studies [12]. A 1-m-long wooden beam (diameter: 20 mm or 10 mm) was placed 50 cm above the table, and a masking plastic box was placed at one of its ends as an endpoint. The starting point was set 75 cm from the goal point. Each mouse was habituated by placing it in a plastic box for 30 s. The mice were allowed to cross the beam 2 times for training before each beam test. Subsequently, the time taken to reach the box from the starting point and the number of slips and falls for each mouse were scored. The test was repeated twice at intervals of 5–10 min.

2.2.5. Foot stamp test

Balance was assessed using mouse gait, as previously described [13]. After painting the limbs of the mice with water-soluble paint, their gait was recorded on white paper. Gait regularity was investigated by comparing and analyzing RA mouse models with normal mice based on the measurements of stride length and width.

2.2.6. Grip-strength test

Balance was evaluated using the grip strength test, as previously described [13]. RA and normal mice were suspended in the supine position on an inverted metal mesh and the duration for which the animal remained on the meshwork was recorded.

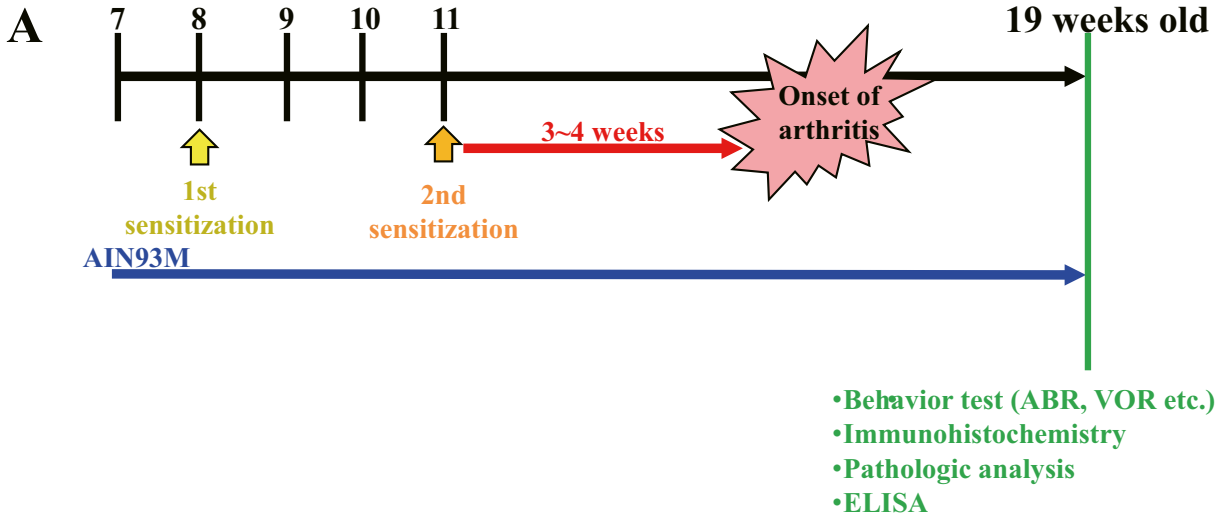

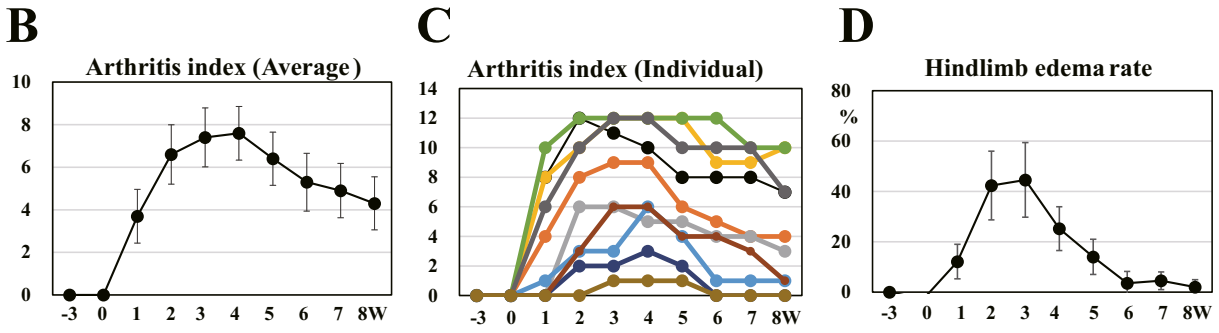

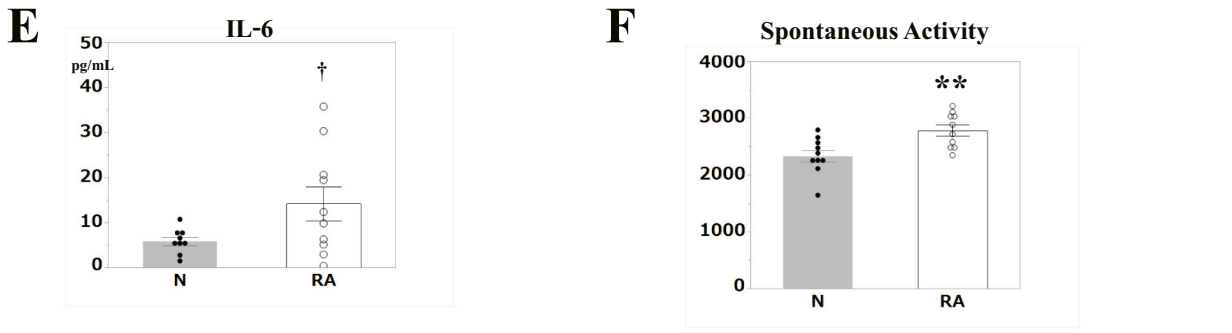

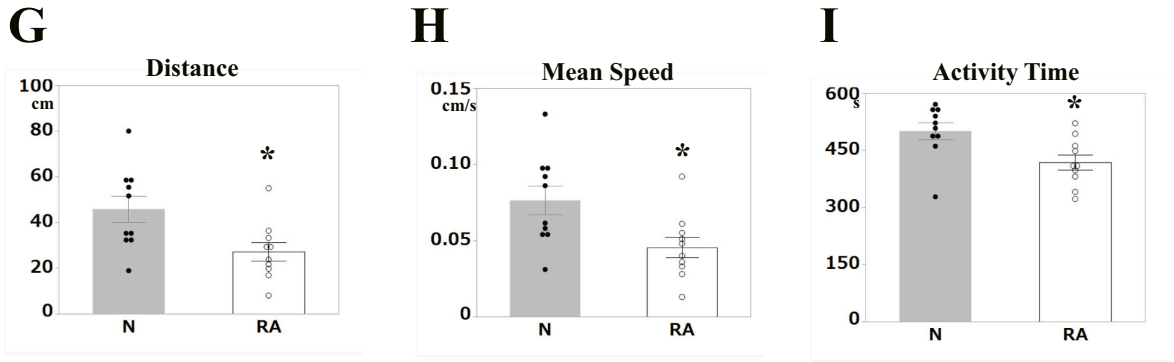

(caption on next page)

Fig. 1. Preparation of the type II collagen-sensitized RA mouse models.
(A) Study design.
(B, C) Line graph of the average (B) and individual values (C) of the arthritis index. Data are expressed as the mean ± SEM of ten mice. X-axis notation: −3 (3 weeks before 2nd sensitization), 0 (on the day of 2nd sensitization) and 1–8 (1–8 weeks after second sensitization).
(D) Line graph of the average hindlimb edema rate. Data are expressed as the mean ± SEM of ten mice. X-axis notation: −3 (3 weeks before 2nd sensitization), 0 (on the day of 2nd sensitization) and 1–8 (1–8 weeks after second sensitization).
(E) Bar graph of average blood levels of IL-6. Data are expressed as the mean ± SEM of ten mice per group. Grey: normal group (N), White: RA group (RA). Data are expressed as the mean ± SEM. $^{\dagger}p < 0.06$ vs. normal mice, determined by Student's paired *t*-test.
(F) Bar graph of average measured value of spontaneous activity. Data are expressed as the mean ± SEM of ten mice per group. Grey: normal group (N), White: RA group (RA). Data are expressed as the mean ± SEM. $^{**}p < 0.01$ vs. normal mice, determined by Student's paired *t*-test.
(G, H, I) Bar graph of average distance (G), mean speed (H), and activity time (I). Data are expressed as the mean ± SEM of ten mice per group. Grey: normal group (N), White: RA group (RA). Data are expressed as the mean ± SEM. $^{*}p < 0.05$ vs. normal mice, determined by Student's paired *t*-test.

2.3. Enzyme-linked immunosorbent assay (ELISA)

Serum samples were obtained from supernatants by the centrifugation (3000 rpm, 10 min, 4 °C) of whole blood collected from the right atrium. IL-6 levels were measured using ELISA kits (Catalog No. SM6000B, R&D Systems Inc., Minneapolis, MN, USA), according to the manufacturer's instructions and calculated based on a standard curve.

2.4. Auditory brainstem response

ABR was performed as described in previous reports [14]. After anesthesia, needle electrodes were inserted into the calvaria and auricle with a grounding electrode at the back. Tucker-Davis Technologies hardware for the ABR (Tucker-Davis Technologies, Alachua, FL, USA) was used for stimulus generation and signal acquisition. We used alternating polarity click stimuli of 100 μs duration, 4, 8, 16, 24 and 32 kHz tones, and bursts with a 0.1 ms linear rise and fall envelope. The duration of the tone bursts was 1 ms. An algorithm for the automated determination of ABR amplitudes based on the definitions provided above was developed by the Bio Research Center (Nagoya, Japan). Thresholds were determined in 5 dB steps of decreasing stimulus intensity until the waveforms lost any reproducible morphologies (from 100 dB to below 5 dB sound pressure level). For each sound level, 1024 responses were averaged. The lack of a positive electroencephalogram at 100 dB was regarded as indicating complete deafness owing to the limit of detection, and 105 dB was used to calculate the average hearing threshold.

2.5. Vestibulo-ocular reflex test

Installation of metal fittings on the mouse head was performed under anesthesia using a mixture of 100 mg/kg ketamine and 10 mg/kg xylazine, with the addition of local anesthesia (1 % lidocaine). A small skin incision was made on the head of the mouse, and a metal plate was fixed with a screw hole in the center of the skull using dental cement (Sun Medical, Shiga, Japan). The mice were followed for 24 h after placement of the metal plates [9]. At the center of the VOR analysis rotator, a metal bar was attached to the forehead via a metal plate. (Fig. 4A, B) [15]. To induce VOR, the rotator was automatically rotated in the dark in a horizontal sinusoidal manner at frequencies of 0.3, 1, and 2 Hz. Photographs of the mouse eyeball and rotating apparatus were captured using two high-speed infrared cameras (240-Hz sampling rate; Sentech, Kanagawa, Japan) (Fig. 4A arrowhead, 4 B arrow, and 4C). The maximum angular velocities were 79.04°, 62.80°, and 62.80°/s. The images of the mouse eyeball and rotator were synchronized using StreamPix software (Nor Pix, Montreal, Canada) (Fig. 4D). All experimental devices (metal plate processing, cylinders, rotating plates, and camera fixtures) were manufactured by Bio-Medica (Osaka, Japan).

The rotator was rotated approximately 7–14 times per analysis, although data were only collected from the 3rd to 5th rotation. Each wavelength was measured once in each mouse. Eye movements during the test were checked using a monitor, and if any abnormal eye movements were observed, the test was repeated.

2.6. Eye movement analysis

Eye movement images were stored in a 645 × 485-pixel jpeg format, and the pupil edge was approximated as an ellipse, according to our own previously-reported method [9,16]. The inertial coordinate frame (*x, y, z*) was defined such that the x-axis was perpendicular to the image plane (positive forward), the y-axis was parallel to the horizontal axis of the image plane (positive left), and the z-axis was parallel to the vertical axis of the image plane (positive upward). On the digital image plane, the eye rotation center (*c*) (0, *ya, za*) was determined as the intersection between the extension of the minor pupil ellipse axes. Furthermore, the rotation radius of the pupil center was computed using Eq. (1):

$$R\sqrt{1-(\text{the length of } \textit{the} \text{ minor axis}/\text{the length of } \textit{the} \text{ major axis})^2} = \text{r} \tag{1}$$

where *r* is the distance between *c* and the center of the pupil ellipse (0, *yb, zb*) [17]. After measuring the *yz* coordinates (*yb, zb*) of the pupil ellipse center on the digital image plane, the 3D coordinates of the pupil center were computed using Eq. (2):

$$\left(\sqrt{R^2-(yb-za)^2-(zb-za)^2}\, yb - yazb - za\right) \tag{2}$$

Finally, the horizontal component of the eye rotation was computed using Eq. (3):

$$arctan\left((yb-ya)\Big/\sqrt{R^2-(yb-ya)^2-(zb-za)^2}\right) \tag{3}$$

2.7. Analysis during the rotation of the rotating table

A 240-Hz high-resolution infrared digital camera (Sentech, Kanagawa, Japan) was placed 30 cm above the rotating table, with the camera axis vertical to the table. The coordinates of the two markers on the rotating table, (*x*t1 and *y*t1) and (*x*t2 and *y*t2), were determined from the table images. The rotating table position was calculated by applying the "atan2" function in Excel software (v. 2010; Microsoft, USA) to the data (atan2 (xt2 -*x*t1, *y*t2 - *y*t1)). The positive direction occurs when the table rotates counterclockwise [9].

2.8. Calculation of VOR gain

Eye and rotating table positions were distinguished, and their angular velocities were computated. We computed the eye velocity [18] and extracted the slow-phase eye velocity (SPEV) of nystagmus using our previously-described method [19,20]. SPEVs were approximated three-dimensionally with the best-fit sine curve using the least-squares method, as follows: V_e sin ($2\pi \cdot 0.5\ t + Pe$), where *Ve* is the maximum angular velocity axis angle. Using the least squares method, the rotating table angular velocity was approximated to the formula $V_t$sin (2πft -α), with the value of *a* obtained when the sign of V_t was positive. Next, using the value of *f* and the least squares method, angular eye velocity was approximated to the formula, $V_e$sin ($2\pi ft$ -β), and the value of β was

determined when V_e was positive. The VOR gain was calculated using the following formula: gain = V_e/V_t.

2.9. Static tilt

All static tilt experiments were performed in the dark. The mouse was placed in a cylindrical plastic container and fixed to the device with a screw using a metal plate attached to its head. The container was fixed to a board which contained a gear with 36 teeth positioned at 10° intervals and meshed at 10° intervals (Fig. 5A). The mouse was fixed to the board in two body positions. In one body position, the mouse was rotated laterally about the roll axis (x-axis). In other body positions, the mouse was rotated back and forth about the pitch axis (Y axis) [21]. The board was manually rotated and held at 0°, 10°, 20°, 30°, 40°, and 50° rotated positions for approximately 10 s. The rotation position was slowly changed (2°/s) for 5 s. The direction of rotation was randomly selected.

The position of the eyeball in the normal position was used as a reference, and the angle of the eyeball that changed when the body was tilted was compared. The vertical component of the eyeball was measured. The movements of both eyeballs were recorded; however, because the angle changed by both eyeballs was the same, the analysis was performed using the right eye. We further analyzed the position at which the eyeballs rested when the body tilt angles were 10°, 30°, and 50°. Otolithic function can be evaluated by comparing the angles of deviation of the eyeballs.

2.10. Eye movement recording

An infrared camera (sampling rate 60 Hz) (GR200HD2-IR, Shodensha Co., Ltd., Osaka, Japan) was used to record the movement of both eyes during tilting under dark conditions. Images of both eyes were acquired using a Color Quad Processor (SG-202II; Daiwa industry, Kanagawa, Japan). Cameras were positioned adjacent to the eyes (Fig. 5A). When recording eye movements in the dark, the pupils were contracted with an ophthalmic solution (1 % pilocarpine hydrochloride; Nippon Tenganyaku Kenkyusho, Nagoya, Japan).

2.11. Recording and analysis of mouse movement

To record mouse movement during tilting in the dark, two markers were set on the board (Fig. 5A), and their movement was recorded using an infrared camera (GR200HD2-IR). The images of the markers were synchronized with the images of the eyes using a color quad processor (SG-202II). The coordinates of the center of gravity of the two markers were then extracted. The tilt angle of the mouse was calculated from the tilt angle of the line connecting the two centers.

2.12. Tissue sample preparation and Hematoxylin-Eosin stain

Mice were fixed by perfusion using a 4 % paraformaldehyde (PFA) fixative under anesthesia with a combined anesthetic (0.3 mg/kg medetomidine, 4.0 mg/kg midazolam, and 5.0 mg/kg butorphanol) [22]. Temporal bones, including the cochlea and semicircular canal, were quickly removed under a microscope (Leica, Wetzlar, Germany), and replaced with cold phosphate-buffered saline (PBS, pH 7.4). The extracted temporal bone was immersed in a 4 % PFA fixative at 4 °C overnight, and then immersed in 10 % EDTA in PBS for a week at 4 °C for decalcification. The vestibular ganglia were removed after perfusion and postfixed using the same fixative. The samples were dehydrated using a series of ascending alcohol concentrations and embedded in paraffin (tissue preparation, T580, FALMA, Tokyo, Japan) using Clear Plus (FALMA). Sections of 5 μm thickness were prepared with a Rotary microtome (Leika), and mounted on MAS-coated glass slides (Matsunami-glass, Osaka, Japan). Samples were stored at 4 °C until use. After deparaffinization, the samples were further deparaffinized with xylene, hydrated through a series of descending alcohol concentrations, and stained with HE solution (FUJIFILM Wako Chemicals Corporation, Osaka, Japan). All stained samples were analyzed using a Keyence microscope (KEYENCE Corporation, Osaka, Japan).

2.13. Phalloidin staining

After fixing with 4 % PFA fixative, the inner ears were decalcified for a week, as described above. Under a microscope, cochlear hair cells were removed from the inner ear and divided into the basal, middle, and apical turns. Each sample was washed with PBS and stained with a rhodamine phalloidin solution (1:500; Catalog No. PHDR1, Cytoskeleton, Denver, Co) for 30 min at 22 ± 2 °C. After thorough washing, all the stained samples were analyzed using a Keyence microscope (KEYENCE Corporation).

2.14. Immunohistochemical detection of collagen type II

Immunohistochemical analysis was performed as previously described [23]. After deparaffinization with xylene, temporal bone samples were hydrophilized using a descending ethanol series. For antigen retrieval, the slides were heated in 0.01 M citrate buffer (pH 6.0) at 95 °C for 40 min, and then immersed in the same solution at 22 ± 2 °C for 20 min. Subsequently, to inhibit non-specific reactions and improve antibody permeability, the slides were immersed in a blocking solution (0.1 M PBS containing 5 % bovine serum albumin and 0.3 % Triton X-100) at 22 ± 2 °C for 30 min. The slides were then treated with anti-collagen type II rabbit polyclonal antibodies (AB-34712, 1:100; Abcam, Tokyo, Japan) and anti-collagen type II rabbit polyclonal antibodies (Cat No. GTX100829, 1:100, Gene Tex, Tokyo, Japan) in the blocking solution at 4 °C overnight. After several washes, the slides were incubated with biotin-conjugated anti-rabbit IgG antibody (1:200; Vector Laboratories, Inc. Burlingame, CA)in PBS at 22 ± 2 °C for 30 min. Next, the slides were treated with 0.3 % H_2O_2 for 30 min at 22 ± 2 °C to inactivate endogenous hydrogen peroxide catabolic enzymes. To sensitize the positive signal, the samples were incubated in an avidin-biotin complex (1:50, VECTOR) in PBS at 22 ± 2 °C for 30 min, which was allowed to react for 30 min in advance. The color reaction was performed using 50 mM Tris-HCl buffered saline containing 10 mg 3,3'Diaminobenzidine (concentration: 10 mg/50 mL; Merck KGaA, Darmstadt, Germany) and 0.01 % H_2O_2. After counterstaining with hematoxylin, dehydrating with ethanol, and clearing with xylene, the samples were mounted in Entellan (Merck). Images were acquired using a Keyence microscope (KEYENCE Corporation).

2.15. Type II collagen autoantibody detection

Under anesthesia, whole blood was collected from the right atria of normal and RA mouse models. The samples were centrifuged (3000 rpm, 10 min, 4 °C), and serum was collected. Samples were stored at −80 °C until use. Type II collagen autoantibody detection in the serum was performed using a serum type II collagen antibody detection kit (Collagen Research Center, Tokyo, Japan), according to the manufacturer's instructions. Optical density (OD) was measured at 450 nm using a microplate reader (SH-9000Lab; HITACHI). Samples with OD values higher than those of the positive control sera were considered positive. The OD value = 1 of the RA mouse models was calculated using the average OD value of the RA mouse models.

2.16. Magnetic resonance imaging (MRI)

Gd MRI contrast agent (0.5 M gadoteridol) was administered intraperitoneally (0.10 mL/20 g body weight) to discriminate the scala vestibuli, scala tympani, and scala media [24]. Sagittal cochlear magnetic resonance images were obtained at 90 min (right side) and 120 min (left side) after Gd administration. In vivo MRI was performed using an 11.7

T vertical bore scanner (AVANCE II 500WB; Bruker BioSpin, Ettlingen, Germany). Anesthesia was initially induced with 2.0 % isoflurane, and maintained with 1.6 % isoflurane during MRI. The body temperatures of mice were maintained at 37 °C with circulating warm water. Ten T_1 weighted sagittal images of each side of the cochlea were obtained using the Rapid Acquisition with Relaxation Enhancement technique [25]. The acquisition parameters were as follows: field of view [FOV] = 20 mm × 20 mm, matrix size = 512 × 512, in-plane resolution = 39 μm, slice thickness = 200 μm, repetition time [TR] = 800 ms, echo time [TE] = 14.8 ms, echo train length = 4, number of averages [NA] = 16, acquisition time [TA] for each cochlea = 27 min.

2.17. Evaluation method of endolymphatic hydrops by inner ear MRI

Endolymphatic hydrops were evaluated as described by Imai et al. [26]. Specifically, the inner ear MRI showing the maximum cochlear axis was magnified 15 times, and the boundaries of the cochlear bone surrounding the endolymphatic and perilymphatic cavities were drawn with lines (Fig. 9A and B).

The number of pixels in the line surrounding the endolymphatic and perilymphatic spaces was calculated, and the ratio was obtained by dividing the number of pixels in the perilymphatic space by the number of pixels in the endolymphatic space. Endolymphatic hydrops were evaluated by comparing the ratio between the normal and RA model groups.

2.18. Statistical analysis

Data are shown as the mean ± SE of experiments between two independent groups. Statistical analysis was performed using the Excel statistical software Statcel 4, and the difference between two groups was determined using Student's *t*-test or the Mann–Whitney *U* test. In all statistical processing, $p < 0.05$ was considered to indicate a significant difference.

2.19. Study approval

All mouse experiments were conducted according to protocols approved by the Committee of Animal Experiments of Osaka University (approval number 02–001-003), and in accordance with the National Institute of Health Guide for the Care and Use of Laboratory Animals. This study was further conducted in compliance with the ARRIVE guidelines. All efforts were made to minimize the number of mice and to decrease anguish. When food and water consumption became difficult, food was placed on the bedding and supplemental agar jelly was provided. Moreover, if abnormalities or hypothetical humane endpoints (for example, difficulty in feeding/watering, breathing problems, self-harm, rapid weight loss of ≥20 % in a few days) were noted in the experimental mice, they were immediately euthanized by intraperitoneal administration of pentobarbital (200 mg/kg).

3. Results

3.1. Establishment of rheumatoid arthritis mouse models

First, we investigated whether mice sensitized to type II collagen developed RA, using an arthritis index. We found that the arthritis index rose sharply until 3 weeks after sensitization, peaked at the 5th week, and gradually decreased thereafter; the arthritis index at the 8th week was approximately the same as at the 1st week (Fig. 1B). The arthritis index peaked at 3–4 weeks in all mice; however, the maximum value varied greatly between mice, ranging from 1 to 12 (Fig. 1C). Hindlimb edema associated with inflammation also showed fluctuations similar to those of the arthritic index. Swelling began rapidly after the 1st week of sensitization, and peaked between weeks 3 and 4. Subsequently, swelling gradually decreased, and almost no edema was observed after the 6th week (Fig. 1D). These results revealed that all type II collagen-sensitized mice developed RA due to type II collagen sensitization.

Subsequently, to investigate the systemic inflammation associated with RA, we analyzed the blood levels of IL-6, an inflammatory cytokine, using ELISA, finding that levels in Type II collagen-sensitized mice tended to increase by approximately 2.5 times compared to that in normal mice (Fig. 1E). ELISA further demonstrated that the RA mouse models showed persistent systemic inflammation associated with RA.

Furthermore, to investigate behavioral changes associated with RA, we measured spontaneous activity and conducted an open-field test. It has previously been reported that RA mouse models exhibit decreased behavioral abilities on the open-field test [27]. Surprisingly, the spontaneous activity of type II collagen-sensitized mice was significantly higher than that of the normal mice (Fig. 1F). In addition, similar to previous reports, in the open field tests, significant decreases in movement distance, movement speed, and activity time were observed in type II collagen-sensitized mice compared with normal mice (Fig. 1G-I). Behavioral tests further revealed that the RA mouse models showed behavioral abnormalities.

Collectively, these results revealed that mice sensitized with type II collagen developed RA and sustained inflammation. In this study, we used type II collagen-sensitized mice as the RA mouse model to analyze hearing and vestibular functions.

3.2. RA mouse models exhibited hearing loss

To investigate whether RA mouse models develop hearing loss, which is the primary symptom of AIED, we measured the hearing threshold of normal and RA mouse models using analysis of the ABR. DBA/1 J mice with RA induced by type II collagen were designated as the RA mouse model (RA) group, while age-matched normal DBA/1 J mice were designated as the normal group. Higher thresholds were observed in RA mouse models than in normal mice at all wavelengths (8 and 16 kHz, $p < 0.05$; 4, 24, 32 kHz, $p < 0.001$; Fig. 2A). Surprisingly, the RA mouse model could not hear at 32 kHz, and only a few mice could not hear at 4 and 8 kHz (Fig. 2B). These results suggest that RA mouse models develop hearing loss owing to structural abnormalities in the inner ear.

3.3. RA mouse model developed lateral semicircular canal dysfunction

Next, we conducted the balance beam, rotarod, and foot stamp tests to examine the presence of vertigo symptoms associated with AIED. These tests are commonly used to detect balance deficits manifesting as postural control, spatial awareness, sensorimotor function, and coordination. The results of the balance beam test showed that the number of slips and falls significantly increased in the RA mouse models in trials with a beam diameter of 10 mm. In trials with a diameter of 20 mm, the RA mouse models tended to fall, but there was no difference in slip between the two groups. Regardless of diameter, the arrival time tended to increase in the RA mouse models (Fig. 3A). In addition, the rotarod test revealed that the duration was significantly decreased in RA mouse models compared to that in normal mice (Fig. 3B). Furthermore, in the foot stamp test, the stride length of each of the four limbs was smaller in the RA mouse models, particularly in the left limbs (Fig. 3C, D). However, there was no significant difference in the width between the left and right sides. Notably, some RA mouse models showed footprints that are tilted to the left and are unable to walk straight. These behavioral test result suggest that RA mouse models have abnormalities in vestibular function. However, RA mouse models show inflammation and pain in the limbs related to arthritis; therefore, the reduced motor function associated with these symptoms may have affected the test results. Therefore, we further measured muscle strength in the limbs of the RA mouse models using a grip strength test. The RA mouse models hung on the wire mesh for approximately half the time as compared to normal mice, while half of the RA mouse models were unable to grasp the wire

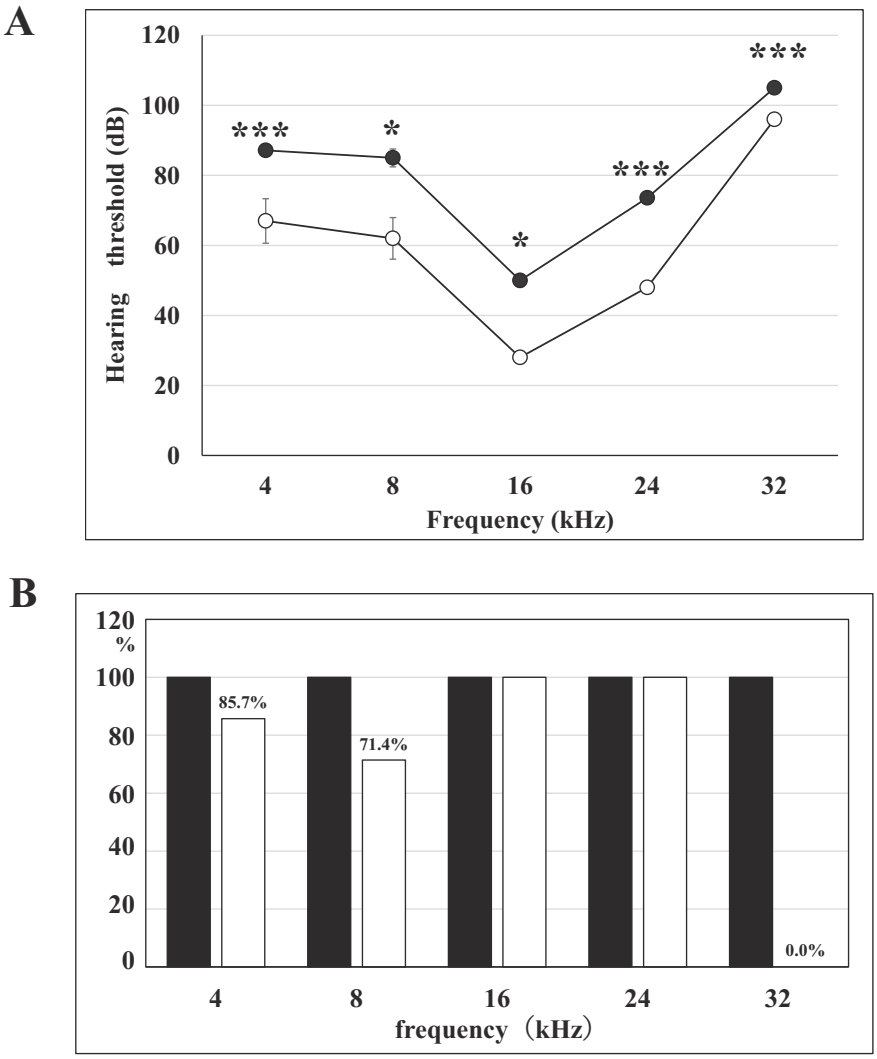

Fig. 2. ABR analysis results for RA mouse models.
(A, B) Line graph of the average values of hearing threshold (A) and a bar graph indicating the percentage of detectable mice (B). White: normal mice ($n = 5$), Black: RA mouse models ($n = 7$). Line up in order of 4, 8, 16, 24 and 32 kHz from the left. Data are expressed as the mean ± SEM. *$p < 0.05$, **$p < 0.01$, ***$p < 0.001$ vs. normal mice, determined by Student's paired *t*-test.

mesh (Fig. 3E). Therefore, it was suggested that a decline in muscle strength, in addition to a decline in vestibular function, but have been a major factor in the deterioration of test performance in RA mouse models.

To examine whether vestibular function is truly decreased in RA mouse models, we performed VOR and Tilt analysis, which can evaluate vestibular function without involving exercise performance. First, we investigated the function of the lateral semicircular canal in RA mouse models using VOR analysis. The function of the lateral semicircular canal was evaluated using the VOR gain when three types of stimuli (0.3, 1.0, and 2.0 Hz) were applied. The VOR gain of the normal group was 0.57 ± 0.022 at 0.3 Hz, 0.59 ± 0.030 at 1.0 Hz, and 0.65 ± 0.036 at 2 Hz (Fig. 4D), whereas the VOR gain of the RA group was 0.58 ± 0.047 at 0.3 Hz, 0.58 ± 0.021 at 1.0 Hz, and 0.55 ± 0.865 at 2 Hz. When the stimulus was applied at 0.3 and 1 Hz, there was no significant difference in the VOR gain between the two groups (0.3 Hz, $p = 0.805$; 1.0 Hz, $p = 0.865$). However, when the stimulus was applied at 2 Hz, a significant decrease in VOR gain was observed in the RA group compared to the normal group ($p = 0.038$; Fig. 4E). Taken together, these results indicated that the lateral semicircular canal function was significantly lower in the RA group than in the normal group.

Subsequently, we evaluated the otolithic organ function in RA mouse models using static tilt. We previously showed that otolith function can be evaluated by comparing the vertical component of the displaced eyeball in a static tilt analysis [21]. In addition, the function of the utricle can be evaluated when the mouse is rotated left and right on the roll axis (X-axis), while the function of the saccule can be evaluated when the mouse is rotated back and forth on the pitch axis (Y-axis). We compared the deviation angles of the eyeballs when the mice were tilted 10°, 30°, and 50°. When the mouse position was rotated clockwise on the roll axis (rightward), the deviation angle of the eyeballs was 3.73 ± 1.028°, 16.03 ± 4.290° and 24.36 ± 5.241° in the normal group when tilted by 10°, 30°, and 50°, respectively. Under the same conditions, the deviation angle of the eyeballs in the RA group were 2.57 ± 0.514°, 10.43 ± 1.503°, and 14.83 ± 1.716°, respectively. There were no significant differences in any deviation angle between the two groups10°, $p = 0.313$; 30°, $p = 0.217$; 50°, $p = 0.088$) (Fig. 5B). When the mouse position was rotated clockwise on the pitch axis (forward), the deviation angle of the eyeball is 3.40 ± 0.669°, 9.76 ± 1.494° and 21.75 ± 2.847° in the normal group when tilted by 10°, 30°, and 50°, respectively. Under the same conditions, the deviation angle of the eyeballs in the RA group were 2.98 ± 1.620°, 10.80 ± 1.850°, and 19.25 ± 2.634°,

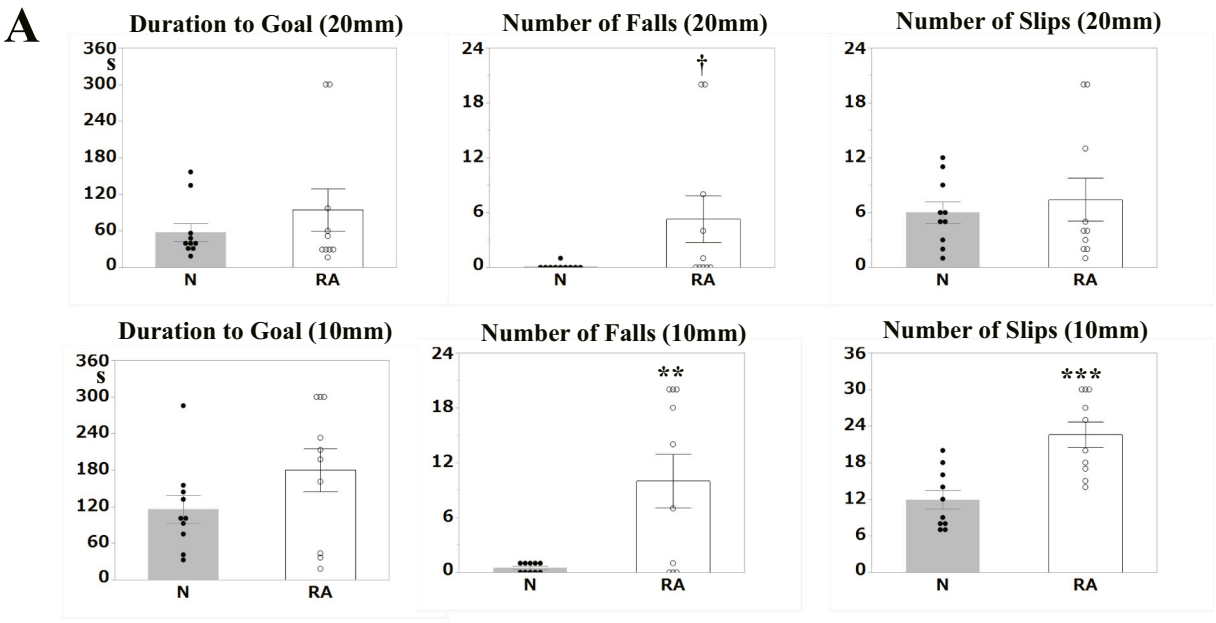

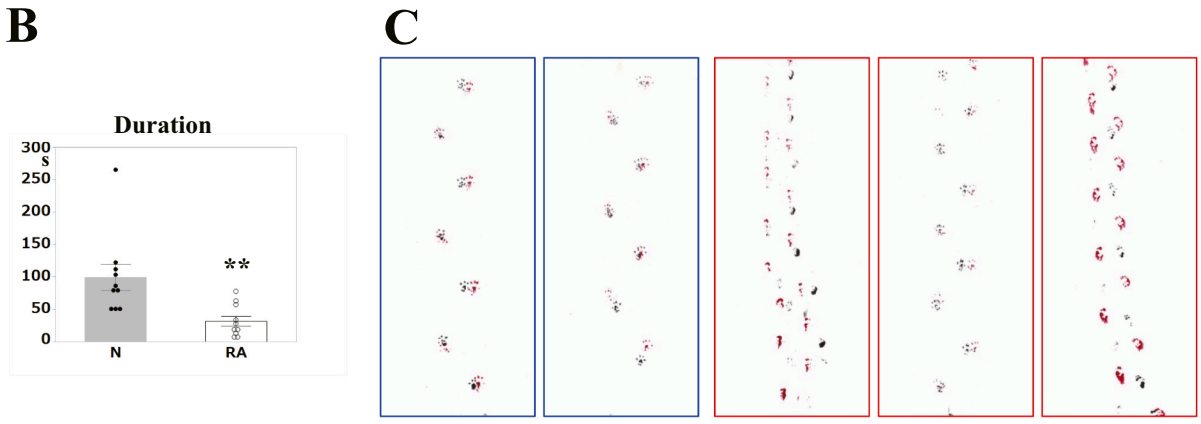

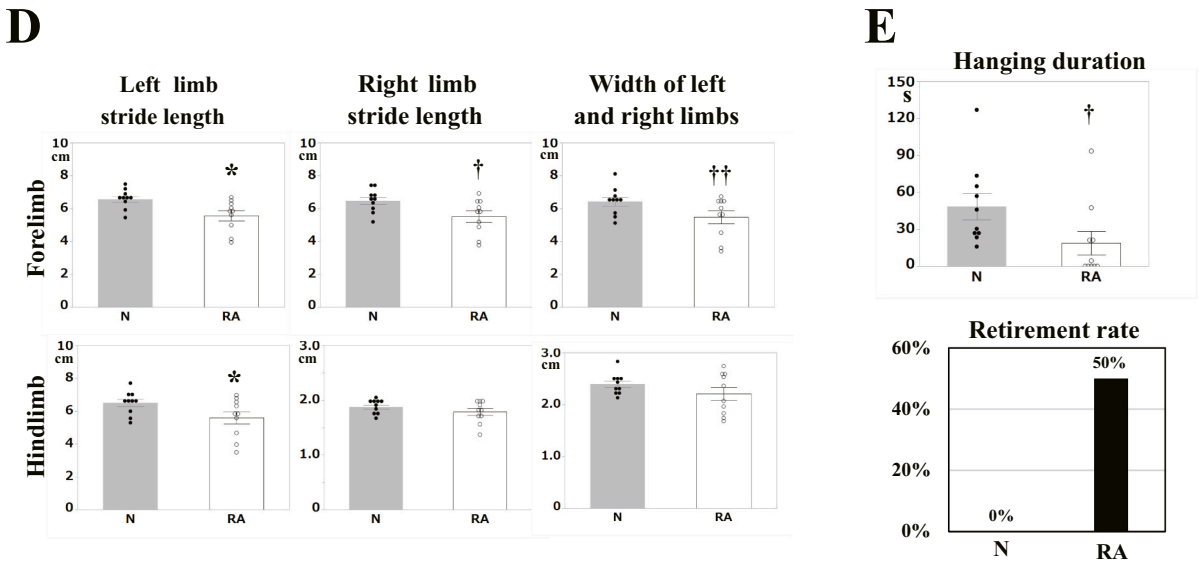

(caption on next page)

Fig. 3. Vestibular function evaluation in RA mouse models using various behavioral tests.
(A) Bar graph of average values of duration to goal (left graphs), number of falls (middle graphs), and number of slips (right graphs) in the balance beam test. 20 mm rod: upper graphs and 10 mm rod: bottom graphs. Grey: normal group (N), White: RA group (RA). Data are expressed as the mean ± SEM of ten mice per group. $^{\dagger}p < 0.06$, $^{**}p < 0.01$, $^{***}p < 0.001$ vs. normal mice, determined by Student's paired *t*-test.
(B) Bar graph of the average duration in the Rotarod test. Grey: normal group (N), White: RA group (RA). Data are expressed as the mean ± SEM of ten mice per group. $^{**}p < 0.01$ vs. normal mice, determined by Student's paired *t*-test.
(C) Representative footprints of normal mice (blue square) and RA mouse models (red square).
(D) Bar graphs of average of left limb stride length (left graphs), right limb stride length (middle graphs), and width of the left and right limbs (right graphs) in the foot stamp test. Forelimb: upper graphs and hindlimb: bottom graphs. Grey: normal group (N), White: RA group ($n = 10$). Data are expressed as the mean ± SEM of ten mice per group. $^{\dagger\dagger}p < 0.07$, $^{\dagger}p < 0.06$, $^{**}p < 0.05$ vs. normal mice, determined by Student's paired *t*-test.
(F) Bar graph of average hanging duration (upper graphs) and retirement rate (immediate fall) (bottom graphs). Data are expressed as the mean ± SEM of ten mice per group. Grey: normal group (N), White: RA group (RA). Data are expressed as the mean ± SEM. $^{\dagger}p < 0.06$ vs. normal mice, determined by Student's paired *t*-test.

respectively. There were no significant differences in any deviation angle between the two groups (10°, $p = 0.819$; 30°, $p = 0.675$; and 50°, $p = 0.531$) (Fig. 5B). When the mouse position was rotated counter-clockwise on the pitch axis (backward), the deviation angle of the eyeball was 3.76 ± 0.951°, 8.58 ± 2.012° and 12.62 ± 2.616° in the normal group when tilted by 10°, 30°, and 50°, respectively. Under the same conditions, the deviation angle of the eyeballs in the RA group were 2.04 ± 0.477°, 8.48 ± 0.943°, and 10.84 ± 0.878°, respectively. There were no significant differences In any deviation angle between the two groups (10°, $p = 0.114$; 30°, $p = 0.965$; and 50°, $p = 0.511$) (Fig. 5B). Taken together, these results suggest there were no significant differences in otolith function between the normal and RA groups.

In summary, although the possibility of decreased function of the otolithic organ cannot be ruled out, our results revealed that vertigo symptoms in RA mouse models were mainly caused by decreased function of the semicircular canal.

3.4. Structural abnormalities of the organ of Corti and the semicircular canal was observed in the RA group

Next, we performed a morphological analysis using hematoxylin and eosin (HE)-stained specimens from the central floor of the cochlea to examine whether there were any abnormalities in the structure of the inner ear. Overall, stria vascularis atrophy was observed in five of the seven mice in the RA group (Fig. 6B, D, 71.4 %), while atrophy of the stria vascularis was not observed in the normal group (Fig. 6A, C). Moreover, the tectorial membrane over the cochlear hair cells in the RA mouse model was thin and fragile compared with that in normal mice (Fig. 6A, B). Subsequently, we analyzed the morphology of the inner ear containing the crista ampullaris of the lateral semicircular canal. Degeneration of nuclei and destruction of the crista ampullaris hair cells were observed in the inner ears of three of the seven mice in the RA group (Fig. 6H-J, 42.9 %). However, such structural destruction was not observed in the inner ear of mice in the normal group (Fig. 6E-G). Furthermore, the loss of sensory hair and eosin-positive internal inflammation of the semicircular canal ampulla were observed in the RA group. Conversely, there were no significant differences in the vestibular ganglia between the control and RA groups (Fig. 6K and L). Taken together, these results revealed that RA mouse models have a disrupted structure of receptors for auditory and vestibular functions in the inner ear.

Subsequently, we performed whole-mount staining of the inner ear to further investigate cochlear hair cells. The results revealed that cochlear hair cells of the basal turn were shed (Fig. 7). However, no significant shedding of the cochlear hair cells was observed in the apical or middle turns. Taken together, the ABR results suggest that the RA mouse models could not hear high-frequency sounds at all because of the loss of hair cells in the basal turn.

In summary, RA mouse models developed hearing loss and decreased vestibular function caused by damage to the organs of Corti and semicircular canals.

3.5. Autoimmune reactions might occur in the inner ear of RA mouse models

To investigate whether the autoimmune reaction against type II collagen antibodies is involved in the structural destruction of the inner ear in the RA mouse models, we examined the localization of type II collagen in the inner ear and the levels of type II collagen autoantibodies in the blood. Immunohistochemistry was performed using two anti-type II collagen antibodies to examine the expression of type II collagen in the inner ear. Positive signals for type II collagen were observed in the spiral ligament, cochlear hair cells, tectorial membrane, membranous labyrinth of the semicircular canals, surrounding bone capsule, and base of the ampullaris (Fig. 8A-C). Furthermore, in the crista ampullaris of the lateral semicircular canal, positive signals were observed at the tips of hair cells, extracellular matrix between hair cells, and base of the crista ampullaris (Fig. 8D, E). In addition, no positive signal was detected in the negative control, confirming the specificity of the antibodies used for immunostaining (Fig. 8F).

Moreover, ELISA revealed that the RA mouse models had increased levels of circulating type II collagen antibodies. The number of autoantibodies was approximately eight times higher in the RA mouse model than in normal mice (Fig. 8G). Taken together, these results suggest that autoimmunity induced by type II collagen antibodies is involved in the structural destruction of the inner ear in mouse models of RA.

3.6. No endolymphatic hydrops was observed in the RA group

Disruption of the stria vascularis has previously been observed in RA mouse models, with one study showing that the stria vascularis is involved in the production and potential of endolymph [27]. Therefore, MRI analysis of the inner ear was conducted to examine whether the RA mouse models had endolymphatic hydrops using a 1500 % magnified MRI image of the largest cochlear axis (Fig. 9A and B). The area ratio of the endolymphatic space (inside the red line frame) to the perilymphatic space (inside the yellow line frame) was calculated and compared between the RA and control groups. The area ratio was 46.6 ± 1.9 % in the RA group and 44.7 ± 2.6 % in the normal group, and there was no difference in the area ratio between the two groups (Fig. 9C).

Taken together, these results suggest that RA mouse models do not exhibit endolymphatic hydrops. It is possible that the decline in hearing and vestibular function may be affected by the structural collapse of each sensory organ.

4. Discussion

In this study, we investigated the course of RA, an autoimmune disease that causes AIED, using mouse models immunized with type II collagen, to clarify the cause of hearing loss and vertigo. Overall, we found that RA mouse models show a significant loss of hearing due to atrophy of the tectorial membrane, shedding of hair cells, and abnormal VOR caused by lateral canal collapse. Moreover, the localization of type II collagen in the organ of Corti and the lateral semicircular canal and the increased type II collagen autoantibody titer suggest that the

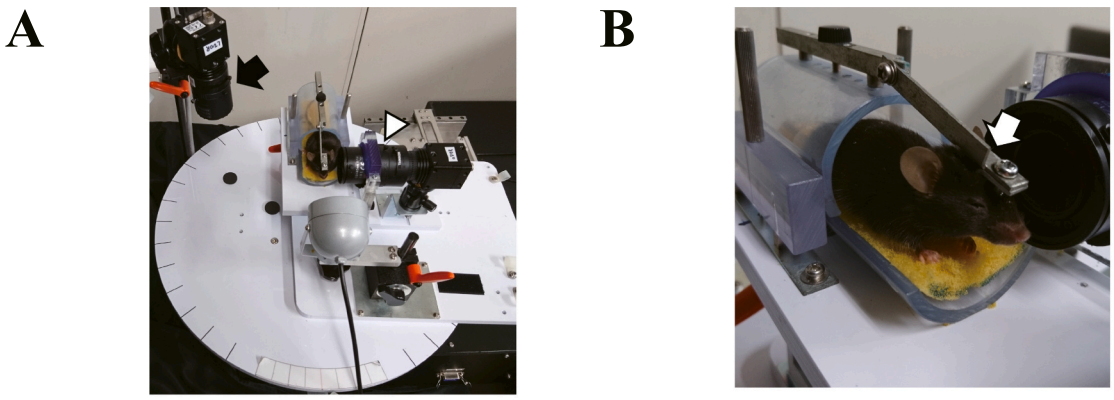

(caption on next page)

Fig. 4. VOR analysis results for RA mouse models.
(A, B) Overview of VOR equipment (A) and the mouse fixture (B). (A) A high-speed (240 Hz) infrared camera was used to photograph the movement of the mouse's left eyeball (arrow) and the movement of the rotating device (black arrow). (B) Arrow: *Z*-shaped metal fixture attached to the mouse head with dental cement. (C) Representative mouse left eyeball during VOR examination in the normal (left) and RA group (right). (D) Representative angular VOR analysis data of the normal group (top) and RA model group (bottom) at 0.3 Hz (left), 1 Hz (middle), and 2 Hz (right). Rough (dot line) and Sin fit data (blue line). (E) The line graph of the mean of VOR in the normal (black circle) and RA group (square) when stimulated at 0.3, 1, and 2 Hz. Data are expressed as the mean ± SEM of seven mice per group. *$p <$ 0.05 vs. normal group, determined by Student's paired *t*-test.

disruption of the organ of Corti and the lateral semicircular canal was due to autoantibodies against type II collagen. We believe that the results of this study will contribute significantly to the development of effective therapeutic agents for AIED.

Similar to previous reports, in this study, we revealed that RA mouse models developed hearing loss, which is the main symptom of AIED (Fig. 2) [28,29]. According to several studies, patients with RA frequently develop hearing loss [30–32]. The RA mouse models showed a loss of cochlear hair cells and shortening of the tectorial membrane (Fig. 6). As the spiral ganglia showed no morphological abnormalities, it was hypothesized that the collapse of the organ of Corti, which is a receptor rather than a nerve transmission system, was largely involved. Furthermore, although the hearing threshold increased at all frequencies, loss of cochlear hair cells was observed only during basal rotation (Fig. 7). Hair cells in the basal turn are involved in hearing high-frequency sounds; therefore, the RA mouse models could not hear sounds at 32 kHz at all (Fig. 2B).

Further, an increase in the threshold was also detected for sounds with frequencies corresponding to apical and mid-rotation, where hair cell shedding was not observed. This suggests that there may be damage to areas other than inner ear hair cells. The first is the tectorial membrane (TM). The tectorial membrane is a membranous extracellular tissue that covers the organ of Corti, and plays an important role along with the basal lamina in the process of cochlear hair cell depolarization due to bending. The RA mouse model exhibited shortening of the tectorial membrane of the organ of Corti (Fig. 6B). Morphological abnormalities in the tectorial membrane affect hearing transmission, suggesting that they may cause hearing loss in RA mouse models.

It is also possible that both the inner and middle ears may be affected. According to previous reports, type II collagen-induced RA mouse models developed hearing loss due to damage to the ear ossicles caused by the inflammation associated with RA [28]. In the RA mouse models, IL-6 levels were elevated in the blood, suggesting that systemic inflammation persisted (Fig. 1E). In addition, clinical studies have revealed that RA patients who develop hearing loss often have significantly higher blood levels of IL-6 than those who do not develop hearing loss [30]. In RA, IL-6 is required for the induction of effector helper T cells (type 17 helper T cells; Th17) involved in joint inflammation [33–35]. The observed sustained increase in IL-6 levels suggests that systemic inflammation is involved in the development of RA-associated hearing loss. In this study, ELISA revealed an increase in IL-6 levels in the blood of RA mouse models, suggesting that the auditory ossicles may be damaged in RA.

It was also shown that sensorineural hearing loss can caused by the collapse of the organ of Corti, such as shedding of hair cells and shortening of the tectorial membrane due to autoimmune reactions. Moreover,

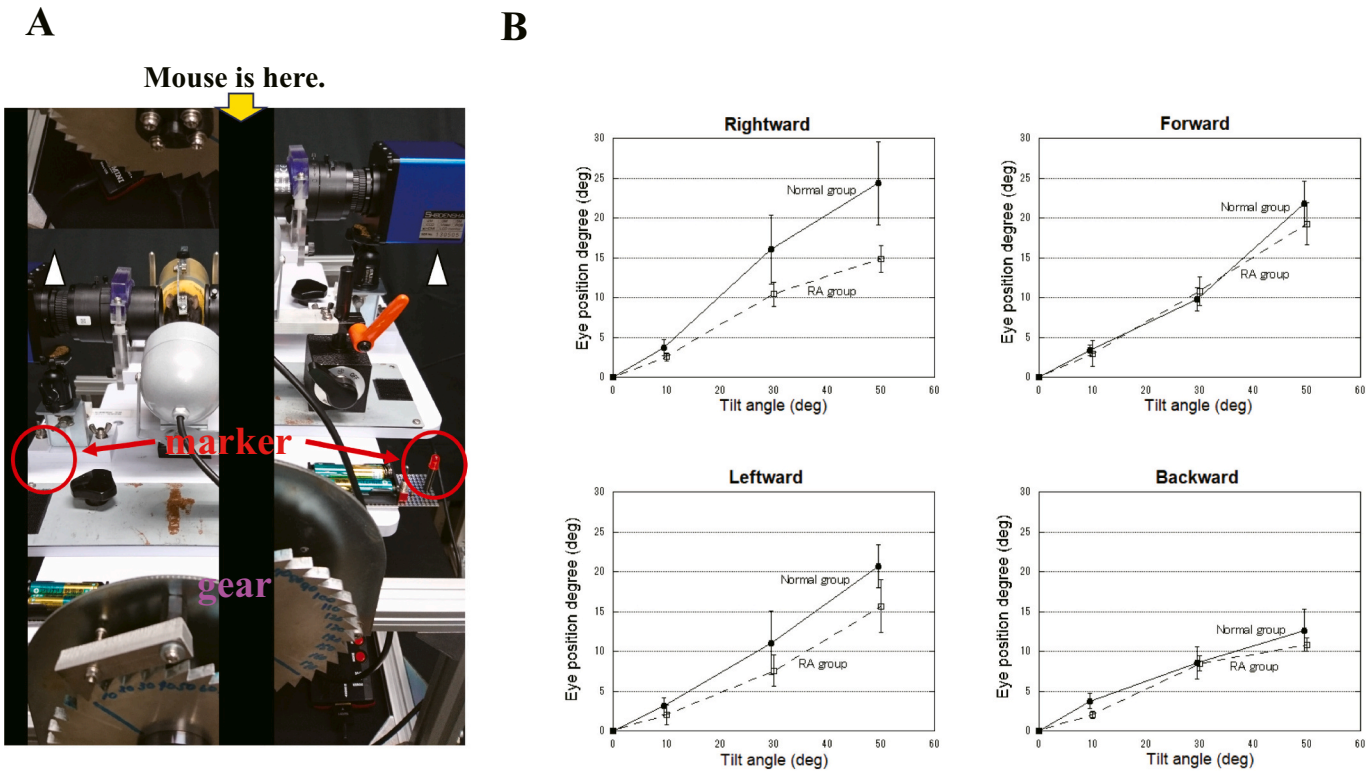

Fig. 5. Tilt analysis results for RA mouse models.
(A) Overview of the static tilt equipment. The gear and container for the stimulation of static tilt in dark conditions. A high-speed (240 Hz) infrared cameras was used to photograph the movement of the mouse's both eyeball (arrow; camera). A Z-shaped metal fixture was attached to the mouse head with dental cement.
(B) The graph shows the deviation angle of the right eyeball when the body position was tilted by 10°, 30°, and 50° in the normal (black circle) and RA group (square). Data are expressed as the mean ± SEM of seven mice per group. *$p < 0.05$ vs. normal group, determined by Student's paired *t*-test.

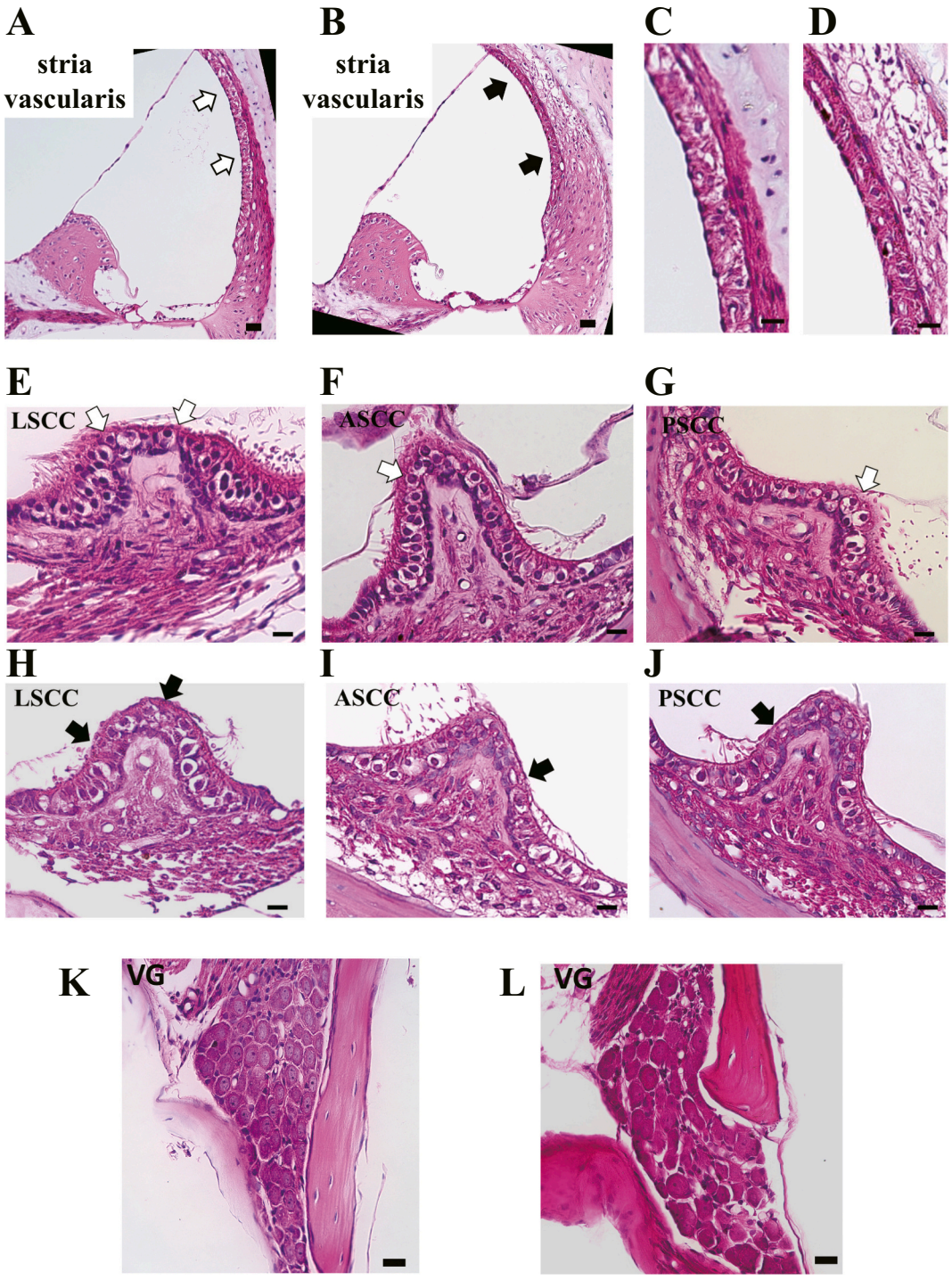

Fig. 6. Pathological analysis using HE staining.
(A-I) Representative examples of H*E*-stained images of the stria vascularis (A-D), the semicircular canal (E-J) and the vestibular ganglion (K, L) in the normal (A, C, E, F G, K; seven mice) and RA group (B, D, H, I, J, L; seven mice). Low magnification (A, B) and high magnification (C, D). (A, B) No atrophied (arrows) and atrophied stria vascularis (black arrows). (E-J) No destructed (E-G: arrows) and destructed semicircular canal hair cells (H-J: black arrows). Lateral (E, H), anterior (F, I) and posterior semicircular canal (G, J). (K, L) No degenerated and atrophied vestibular ganglion cells of both group. LSCC: lateral semicircular canal. ASCC: anterior semicircular canal. PSCC: posterior semicircular canal. VG; vestibular ganglion. Scale bar: 40 μm (A, B), 20 μm (C-L).

an increase in the threshold for sounds at frequencies in areas where hair cells were not shed was observed and the blood level of IL-6 was high, suggesting that conductive hearing loss caused by the collapse of ear ossicles in the middle ear may also develop. In the future, it will be necessary to investigate the middle ear in RA mouse models in detail to further explore the causes of hearing loss. Taken together, these results suggested that RA mouse models develop hearing loss caused by various factors.

In addition to hearing low, AIED may present as vestibular dysfunction, such as vertigo; however, there have been no reports evaluating vestibular function in animal models of type II collagen-induced RA. We investigated vertigo symptoms in an RA mouse models using several behavioral tests to analyze vestibular function. In our study, the results of the balance beam, rotarod, and foot stamp tests revealed that vestibular function was impaired in the RA mouse model

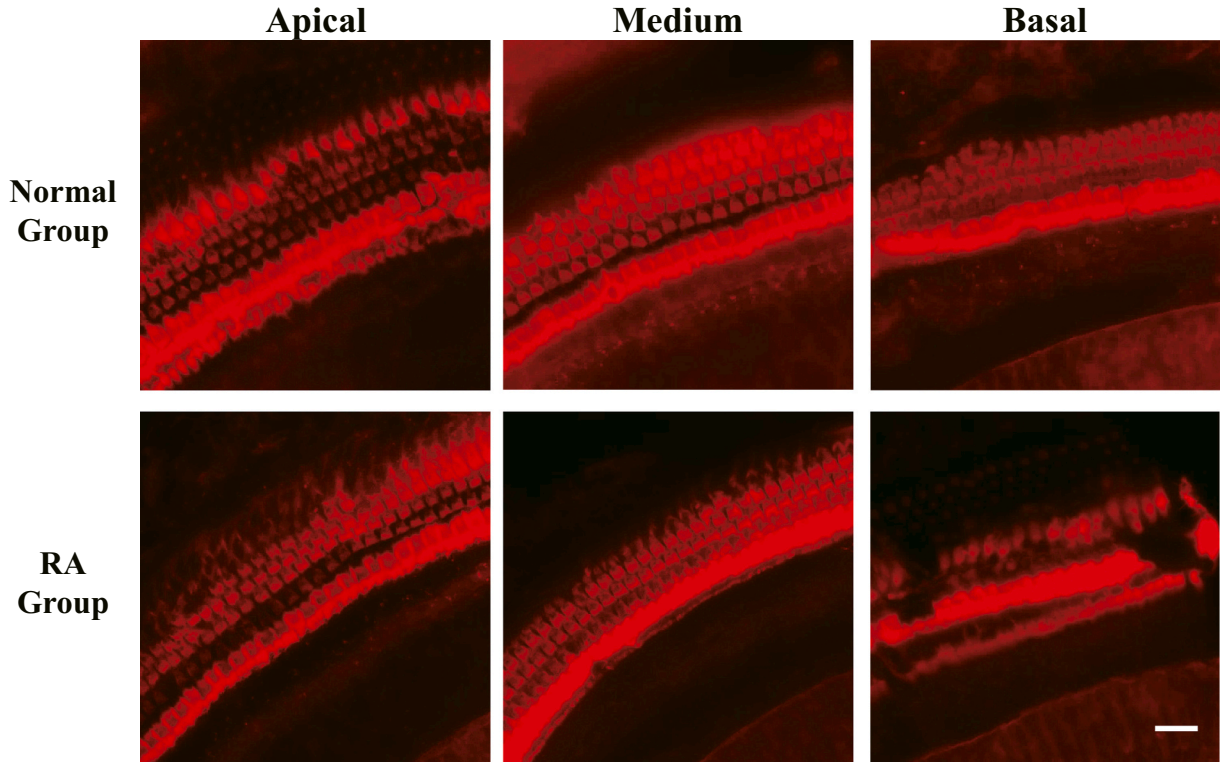

Fig. 7. analysis of the cochlea hair cells in the inner ear.
Representative examples of phalloidin-stained cochlear hair cells in the apical (left panels), medium (middle panels), and basal turns (right panels). Upper: Normal group (ten mice); bottom: RA group (ten mice). Scale bar: 20 μm.

(Fig. 3A-D). Since vestibular function is required for spatial comprehension, posture maintenance, and motor coordination, it is certainly possible to evaluate vestibular function; however, motor function also affects the results, meaning it is difficult to grasp only the state of vestibular function. In fact, the RA mouse models in our study showed decreased muscle strength and behavioral performance (Fig. 3F). Therefore, the behavioral test results mentioned earlier can be attributed to two factors: decreased vestibular function and decreased motor function. Therefore, it is very important to evaluate vestibular function alone, without involving exercise, to understand vertigo symptoms in RA mouse models.

In our previous work, we developed a device that can evaluate VOR function by measuring eye movements generated when mice are rotated and have reported results of VOR using the device to date [16,21]. The advantage of the VOR is that the body of the mouse is fixed in the device; therefore, only the vestibular function can be evaluated. In the present study, the VOR gain in the RA group was found to be lower than that in the control group when stimulation was applied at a frequency of 2 Hz; however, there was no difference in the VOR gain between the two groups when stimulation was applied at a frequency of 0.3 and 1 Hz (Fig. 4E). Hence, the RA mouse model showed decreased semicircular canal and VOR functions against high-frequency stimulation only when high-frequency rotation was used.

In addition, otolith function was evaluated using the static tilt. Similar to the VOR analysis, as the mouse is fixed in the device, otolith function can be evaluated without being affected by motor ability. Previously, we demonstrated that otolith function can be evaluated by comparing the vertical component of the eyeball that occurs when a mouse is tilted [21]. The mice were rotated on the roll and pitch axes to evaluate the utricle and saccule functions, respectively; however, there were no significant differences between the RA and normal groups (Fig. 5). VOR and Tilt analyses revealed that semicircular canal dysfunction was the primary cause of vertigo in RA mouse models. However, the maximum tilt used in the tilt test was 50°, and the gravitational acceleration on the mouse was 0.7 G, which was a weak load, meaning that deterioration in otolith organ function may not have been detected. The fact that the gait of some RA mouse models was curved to the left in the foot stamp test also suggests that otolithic organ function may be impaired in RA mouse models (Fig. 3C). It is important to develop a highly sensitive tilt analysis to accurately determine the functional state of otolith organs.

Herein, we analyzed the structure of the inner ear to investigate the cause of vertigo. Because RA guinea pig models also show structural abnormalities in hair cells in the crest ampulla of the semicircular canal, Yoo et al. speculated that the collapse of the crest ampulla of the semicircular canal causes vertigo [36]. Similar to previous reports, in RA mouse models, nuclear degeneration and collapse of hair cells were observed in the crista ampullaris of the anterior, posterior, and lateral semicircular canals (Fig. 6H-J), whereas no structural abnormalities were observed in the normal group (Fig. 6E-G). Moreover, the vestibular ganglion was confirmed; however, no abnormalities were observed in either group (Fig. 6K and L). These results revealed abnormalities in receptors, but not in transduction pathways, associated with vestibular function. In this study, we observed a loss of hair cells in the crests of the anterior, posterior, and lateral semicircular canal ampulla, suggesting that structural disruption of the crest of the ampullary canal is one of the factors that causes vertigo.

Yoo et al. speculated that damage caused by the deposition of immune complexes on type II collagen present in the inner ear of an RA model caused the onset of AIED [37]. Therefore, we hypothesized that disruption of the inner ear in RA mouse models is caused by a similar mechanism. Reportedly, type II collagen in the inner ear is localized in the tectorial membrane over the cochlear hair cells, the spiral prominence, the semicircular canal membranous labyrinth, the surrounding bone bursa, and the base of the crest of the ampullary [38,39]. Our immunostaining results confirmed the localization of type II collagen in

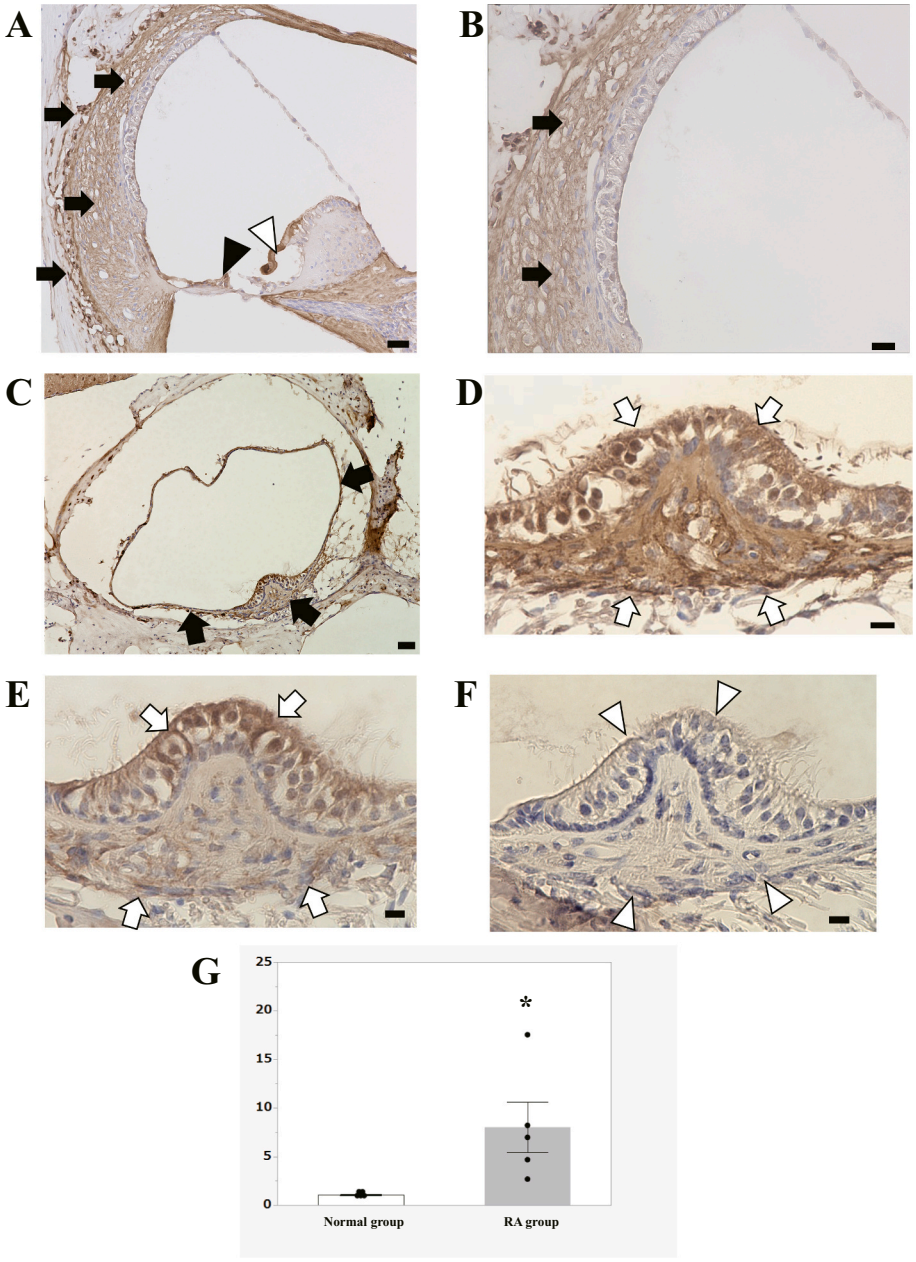

Fig. 8. Localization of type II collagen in the inner ear.
(A-E) Representative samples of type II collagen-stained images of the cochlear duct (A, B), the semicircular canal (C-E). (A, B) The positive signals detected in the stria vascularis (black arrows), auditory hair cell of the cochlear duct (black arrow head), and the tectorial membrane (arrow head). (C-E) The positive signals detected in the membranous labyrinth of the semicircular canal, the surrounding bone capsule (black arrows), and the base of the crest of the ampulla (arrows). Low magnification (A, C) and high magnification (B, D, E). Anti-type II collagen antibodies from Abcam (A-D) and Gentex (E). (F) Negative control images treated with the absence of the primary antibody. Non-stained outer semicircular canal hair cells (arrowheads). Scale bar: 40 μm (A, C), 20 μm (B, D, E, F). (G) The bar chart indicates the mean type II collagen antibody levels using ELISA. White: normal mice. Black: RA mouse model. Data are expressed as the mean ± SEM of five mice per group. *$p < 0.05$ vs. normal mice, determined using Student's paired *t*-test.

the semicircular canal membranous labyrinth, tectorial membrane, spiral ligament, surrounding bone bursa, and the tissue at the base of the crest of the ampulla, as previously reported (Fig. 8A-C). Surprisingly, both cochlear hair cells and hair cells of the lateral semicircular canal ampulla were positive for type II collagen (Fig. 8A, D, E). Although Zoe et al. have previously reported that cochlear inner hair cells express Col2a, which is involved in type II collagen synthesis [40], whether type II collagen is present in the ampulla crest of the lateral semicircular canal remains unclear. The inner hair cells in the organ of Corti contain sensory hair; when mechanically stimulated by sound, the hair bends to generate electrical signals [41]. In contrast, hair cells in the crista ampullaris of the semicircular canal have sensory hairs that bend and generate electrical signals when stimulated by body movements [42]. Because these inner ear hair cells have similar structures and properties, if the Col2a gene is expressed in the hair cells of the organ of Corti, there is a high possibility that the Col2a gene is also expressed in the hair cells of the crista ampullae of the semicircular canals. In fact, in our analysis, we found that type II collagen was also localized at the tip of hair cells on the crest of the lateral semicircular canal ampulla (Fig. 8D, E).

Collagen maintains cell structure, intercellular adhesion, and information transmission [43]. Type II collagen, which is localized in hair cells of the crest of the ampulla of the lateral semicircular canals, plays a

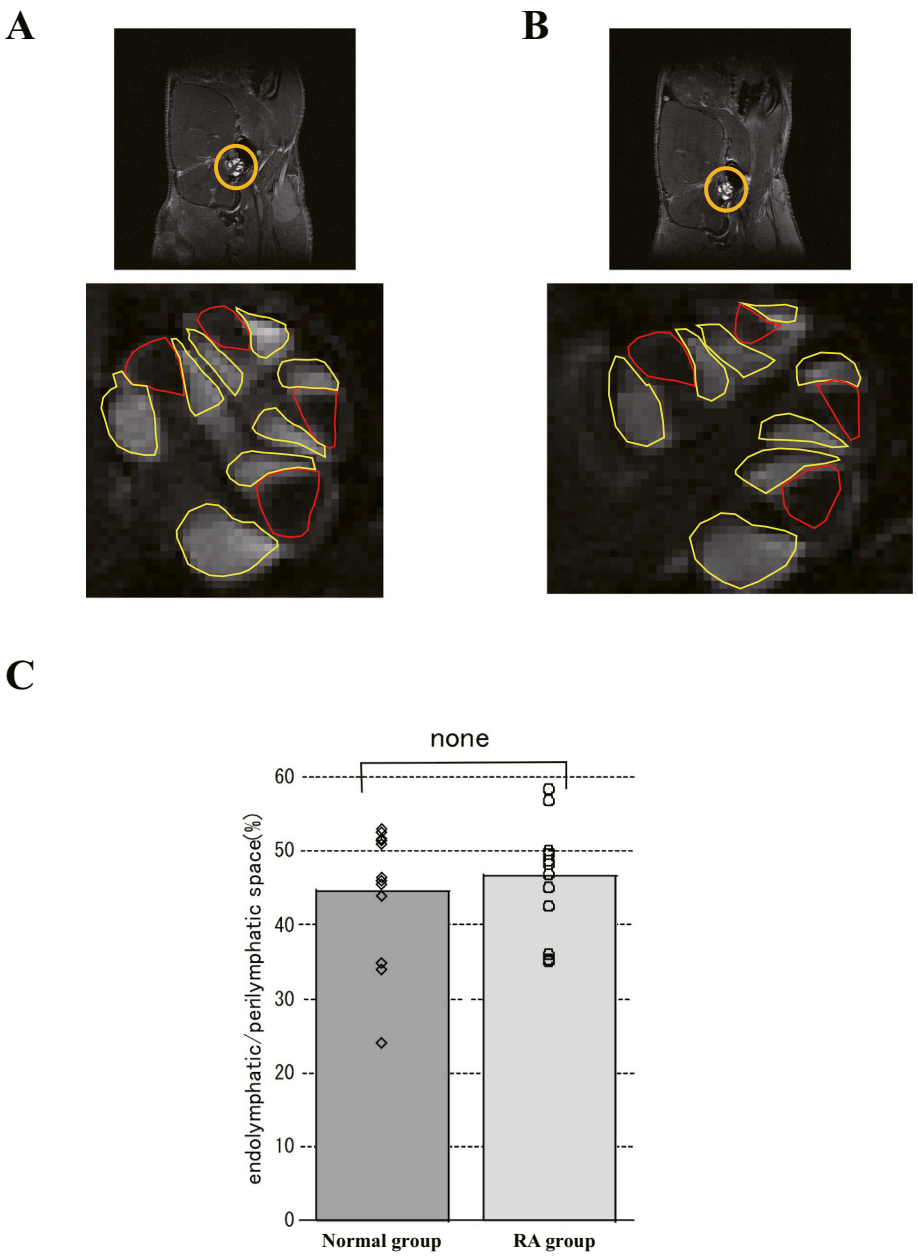

Fig. 9. Evaluation of endolymphatic hydrops using MRI analysis.
(A, B) Representative examples of MRI images in the normal group (A) and the RA model group (B). The upper row is the actual size, and the lower row is a 15× image for evaluation. Yellow and red lines indicate the perilymphatic and endolymphatic space, respectively.
(C) Bar graph of the ratio of endolymphatic/perilymphatic space. To evaluate the endolymphatic hydrops, the ratio (%) of endolymphatic/perilymphatic space pixel count was calculated. The ratio was 46.6 % (SEM ± 1.9 %) in the RA model group and 44.7 % (SEM ± 2.6 %) in the normal group. Mann–Whitney *U* test showed $p = 0.5593$ ($p > 0.05$), indicating no difference in the ratio of endolymphatic space to perilymphatic space and no endolymphatic hydrops. Data are expressed as the mean ± SEM of seven mice per group. None: no significance.

role in maintaining cell structure and intercellular adhesion. Type II collagen was localized in cochlear hair cells and hair cells of the crista ampullaris of the lateral semicircular canal (Fig. 8A-F). Moreover, autoantibodies against type II collagen in the blood were found to be significantly elevated in RA mouse models (Fig. 8G). Considering these results, the deposition of immune complexes against type II collagen may induce the destruction of cochlear and lateral semicircular canal hair cells. Since Harada et al. showed that guinea pig endolymph contains IgG antibodies, complement, and IgG Fc receptors [44], immune complexes may be present in the endolymphatic cavity of type II collagen-induced RA mouse models. Hence, immune complexes adhere to type II collagen at the tip of the cochlear hair cells, stria vascularis, and lateral hair cells of the crista ampullaris of the lateral semicircular canal in the endolymphatic space and induce inflammation. Overall, these results suggest that autoimmune inflammation of type II collagen may lead to the disruption of hearing and balance receptors, causing hearing loss and vestibular dysfunction.

In addition, we considered other possible causes of hearing loss and decline in vestibular function. For example, phagocytosis of macrophages activated by autoreactive effector helper T cells is also thought to be a factor in the collapse of the inner ear structures. However, immunostaining revealed no infiltration of macrophages or microglia in the inner ear (Supplementary Fig. 1). Autoimmune tissue damage in the inner ear involves humoral and cell-mediated mechanisms. In the inner

ear, the immune response develops in the endolymphatic sac, an important organ for immune processing and regulation. The spiral modiolar vein adjacent to the scala tympani is thought to be the initial site of lymphocyte entry into the inner ear, passing through the blood-labyrinthine barrier and reaching the endolymphatic sac [45–47]. Chronic activation of autoreactive lymphocytes against self-proteins within the inner ear destroys sensory cells within the inner ear. It is unclear why autoimmune reactions in joints also occur in the inner ear; however, it is thought that autoreactive lymphocytes circulating throughout the body are induced in the inner ear by certain factors. It has previously been reported that 82 % of patients were accompanied by high-pitched sensorineural hearing loss [48], while stria vascularis destruction has been observed in 71.4 % of RA mouse models. Based on these findings, lymphocyte infiltration may have occurred.

Endolymphatic hydrops also plays a major role in the onset of hearing loss and symptoms of vertigo. In one study, Yoo et al. reported that a guinea pig model of RA exhibited type II collagen-induced endolymphatic hydrops [8]. Magnetic resonance imaging (MRI) enables the clinical evaluation of endolymphatic hydrops [49], and many studies on the mouse inner ear using MRI have been reported [50]. Thus, in this study, we also examined the presence of endolymphatic hydrops using MRI; however, no difference in the endolymphatic space/perilymphatic space ratio between the RA model and normal groups was noted, and no endolymphatic hydrops were observed in the RA mouse models (Fig. 9C). According to Yoo et al., RA animal models (mice, rats, chinchillas, rabbits, monkeys, gerbils, and cats) were prepared by treatment with type II collagen; however, endolymphatic hydrops were only observed in guinea pigs [29]. The reason for this incidence is unknown. Nonetheless, our experimental results are consistent with previous findings that endolymphatic hydrops are not observed in RA mouse models, suggesting that the cause of hearing loss and vestibular dysfunction in RA mouse models is not endolymphatic hydrops. Surprisingly, stria vascularis atrophy and spiral ligament destruction were observed in the RA model group (Fig. 6B and D). As the stria vascularis is involved in endolymph production and potential, structural abnormalities can affect endolymph homeostasis [51]. The temporal bone studies of some patients with AIED have reported atrophy of the stria vascularis [52]. Taken together, these findings show that although endolymphatic hydrops did not develop in the RA group, endolymphatic fluid homeostasis may be abnormal.

In this study, we revealed that inner ear tissue destruction, caused by an autoimmune reaction against type II collagen present in the inner ear, causes both auditory and vestibular dysfunction in RA mouse models. Moreover, RA mouse models have shown atrophy of the stria vascularis in patients with AIED. Therefore, the type II collagen-induced RA mouse models accurately reflect the pathology of AIED. Finally, prior research has shown that Meniere's disease causes symptoms of vertigo, such as AIED, and some symptoms show abnormalities in the immune system [53]. As the symptoms of AIED are similar to those of Meniere's disease, it is often difficult to differentiate between the two diseases, resulting in delays in appropriate treatment. The longer the period without treatment, the worse the tissue damage. Therefore, there is an urgent need to develop tests that will lead to early treatment and effective therapeutic drugs [54]. We believe that the results of this research will contribute to the further analysis of pathological conditions and the development of effective therapeutic drugs in the future.

4.1. Limitations

Although we found evidence of an increase in the serum levels of autoantibodies against type II collagen, localization of type II collagen in the inner ear, and collapse of the inner ear, we were unable to produce any direct evidence to show that antibodies attack the inner ear; therefore, we cannot conclusively state that an autoimmune reaction occurs in the inner ear.

5. Conclusions

Overall, the present study found the following results:

- RA mouse models exhibited shortening of the tectorial membrane, loss of cochlear hair cells, collapse of the ampulla of the third semicircular canal, and atrophy of the stria vascularis, resulting in hearing loss and decreased vestibular function.
- Type II collagen was localized in the sensory receptors for hearing and balance, including in cochlear hair cells, the tectorial membrane, the membranous labyrinth of the semicircular canals, the base of the ampullae of the semicircular canals, and the crista ampullaris hair cells of the ampullae.
- Blood levels of autoantibodies against type II collagen were significantly increased in RA mouse models.
- RA mouse models did not develop endolymphatic hydrops.
- RA mouse models are a useful AIED model mouse that reflects the pathology of AIED.

Supplementary data to this article can be found online at https://doi.org/10.1016/j.bbadis.2024.167198.

Funding details

This research was supported by Center of Innovation Program (COI Program) Grant Number JPMJCE1310, JST Japan and JSPS KAKENHI (No. 21K09654 and No. 23K15862.

CRediT authorship contribution statement

Shotaro Harada: Conceptualization, Data curation, Formal analysis, Funding acquisition, Investigation, Methodology, Visualization, Writing – original draft. **Yoshihisa Koyama:** Conceptualization, Data curation, Formal analysis, Investigation, Methodology, Project administration, Validation, Visualization, Writing – original draft, Writing – review & editing. **Takao Imai:** Data curation, Software, Visualization, Writing – review & editing. **Yoshichika Yoshioka:** Data curation, Methodology, Software, Visualization, Writing – review & editing. **Takuya Sumi:** Formal analysis, Methodology, Visualization, Writing – review & editing. **Hidenori Inohara:** Supervision, Validation, Writing – review & editing. **Shoichi Shimada:** Funding acquisition, Supervision, Validation, Writing – review & editing.

Declaration of competing interest

The authors declare that they have no known competing financial interests or personal relationships that could have appeared to influence the work reported in this paper.

Data availability

No data was used for the research described in the article.

Acknowledgments

This research was supported by the Center of Innovation Program (COI Program, Grant Number JPMJCE1310, JST Japan, and JSPS KAKENHI (Nos. 21K09654 and 23K15862). We thank Ms. M. Hasegawa for technical assistance. We would like to thank Editage (www.editage.com) for English language editing and the Center for Medical Research and Education, Graduate School for Medicine, Osaka University, for technical support.

References

[1] B.F. McCabe, Autoimmune sensorineural hearing loss, Ann. Otol. Rhinol. Laryngol. 88 (1979) 585–589.
[2] A. Ciorba, V. Corazzi, C. Bianchini, C. Aimoni, S. Pelucchi, P.H. Skarzynski, et al., Autoimmune inner ear disease (AIED): A diagnostic challenge, Int. J. Immunopathol. Pharmacol. 32 (2018) 2058738418808680.
[3] J.T. Roland, Autoimmune inner ear disease, Curr. Rheumatol. Rep. 2 (2000) 171–174.
[4] G.S. Firestein, Evolving concepts of rheumatoid arthritis, Nature 423 (2003) 356–361.
[5] T.Y.K. Tomoda, T. Kumazawa, T.J. Yoo, Type II collagen distribution in the middle and ear: – immunohistochemical studies, Ear Research Japan 15 (1984) 199–202.
[6] D.E. Trentham, A.S. Townes, A.H. Kang, Autoimmunity to type II collagen an experimental model of arthritis, J. Exp. Med. 146 (1977) 857–868.
[7] P.H. Wooley, H.S. Luthra, J.M. Stuart, C.S. David, Type II collagen-induced arthritis in mice. I. Major histocompatibility complex (I region) linkage and antibody correlates, J. Exp. Med. 154 (1981) 688–700.
[8] T.J. Yoo, Y. Yazawa, K. Tomoda, R. Floyd, Type II collagen-induced autoimmune endolymphatic hydrops in guinea pig, Science 222 (1983) 65–67.
[9] T. Imai, Y. Takimoto, N. Takeda, A. Uno, H. Inohara, S. Shimada, High-speed video-oculography for measuring three-dimensional rotation vectors of eye movements in mice, PLoS One 11 (2016) e0152307.
[10] F.D. Wood, C.M. Pearson, A. Tanaka, Capacity of mycobacterial wax D and its subfractions to induce adjuvant arthritis in rats, Int. Arch. Allergy Appl. Immunol. 35 (1969) 456–467.
[11] Y. Kobayashi, R. Imamura, Y. Koyama, M. Kondo, H. Kobayashi, N. Nonomura, et al., Renoprotective and neuroprotective effects of enteric hydrogen generation from Si-based agent, Sci. Rep. 10 (2020) 5859.
[12] Y. Takimoto, Y. Ishida, M. Kondo, T. Imai, Y. Hanada, Y. Ozono, et al., P2X(2) receptor deficiency in mouse vestibular end organs attenuates vestibular function, Neuroscience 386 (2018) 41–50.
[13] X. Zhao, S.M. Jones, E.N. Yamoah, Y.W. Lundberg, Otoconin-90 deletion leads to imbalance but normal hearing: a comparison with other otoconia mutants, Neuroscience 153 (2008) 289–299.
[14] Y. Hanada, Y. Nakamura, Y. Ozono, Y. Ishida, Y. Takimoto, M. Taniguchi, et al., Fibroblast growth factor 12 is expressed in spiral and vestibular ganglia and necessary for auditory and equilibrium function, Sci. Rep. 8 (2018) 11491.
[15] D.R. Calabrese, T.E. Hullar, Planar relationships of the semicircular canals in two strains of mice, J. Assoc. Res. Otolaryngol. 7 (2006) 151–159.
[16] Y. Takimoto, T. Imai, M. Kondo, Y. Hanada, A. Uno, Y. Ishida, et al., Cisplatin-induced toxicity decreases the mouse vestibulo-ocular reflex, Toxicol. Lett. 262 (2016) 49–54.
[17] T. Imai, N. Takeda, M. Morita, I. Koizuka, T. Kubo, K. Miura, et al., Rotation vector analysis of eye movement in three dimensions with an infrared CCD camera, Acta Otolaryngol. 119 (1999) 24–28.
[18] T. Haslwanter, Mathematics of three-dimensional eye rotations, Vis. Res. 35 (1995) 1727–1739.
[19] M. Arzi, M. Magnin, A fuzzy set theoretical approach to automatic analysis of nystagmic eye movements, IEEE Trans. Biomed. Eng. 36 (1989) 954–963.
[20] K. Naoi, K. Nakamae, H. Fujioka, T. Imai, K. Sekine, N. Takeda, et al., Three-dimensional eye movement simulator extracting instantaneous eye movement rotation axes, the plane formed by rotation axes, and innervations for eye muscles, IEICE Trans. Inf. Syst. 86 (2003) 2452–2462.
[21] S. Harada, T. Imai, Y. Takimoto, Y. Ohta, T. Sato, T. Kamakura, et al., Development of a new method for assessing otolith function in mice using three-dimensional binocular analysis of the otolith-ocular reflex, Sci. Rep. 11 (2021) 17191.
[22] S. Kawai, Y. Takagi, S. Kaneko, T. Kurosawa, Effect of three types of mixed anesthetic agents alternate to ketamine in mice, Exp. Anim. 60 (2011) 481–487.
[23] Y. Koyama, Y. Kobayashi, I. Hirota, Y. Sun, I. Ohtsu, H. Imai, et al., A new therapy against ulcerative colitis via the intestine and brain using the Si-based agent, Sci. Rep. 12 (2022) 9634.
[24] S.A. Counter, B. Bjelke, E. Borg, T. Klason, Z. Chen, M.L. Duan, Magnetic resonance imaging of the membranous labyrinth during in vivo gadolinium (Gd-DTPA-BMA) uptake in the normal and lesioned cochlea, Neuroreport 11 (2000) 3979–3983.
[25] J. Hennig, A. Nauerth, H. Friedburg, RARE imaging: a fast imaging method for clinical MR, Magn. Reson. Med. 3 (1986) 823–833.
[26] T. Imai, S. Nishiike, K. Oshima, H. Tanaka, Y. Tsuruta, Y. Tomiyama, The resected area of the posterior wall of the external auditory canal during transcanal endoscopic ear surgery for cholesteatoma, Auris Nasus Larynx 44 (2017) 141–146.
[27] A.L. Mausset-Bonnefont, M. Cren, R. Vicente, J. Quentin, C. Jorgensen, F. Apparailly, et al., Arthritis sensory and motor scale: predicting functional deficits from the clinical score in collagen-induced arthritis, Arthritis Res. Ther. 21 (2019) 264.
[28] R. Chen, M. Schwander, M.F. Barbe, M.M. Chan, Ossicular bone damage and hearing loss in rheumatoid arthritis: a correlated functional and high resolution morphometric study in collagen-induced arthritic mice, PLoS One 11 (2016) e0164078.
[29] T.J. Yoo, R.A. Floyd, N. Sudo, T. Ishibe, T. Takeda, K. Tomoda, et al., Factors influencing collagen-induced autoimmune ear disease, Am. J. Otolaryngol. 6 (1985) 209–216.
[30] M. Takatsu, M. Higaki, H. Kinoshita, Y. Mizushima, I. Koizuka, Ear involvement in patients with rheumatoid arthritis, Otol. Neurotol. 26 (2005) 755–761.
[31] M.H. Baradaranfar, A. Doosti, A survey of relationship between rheumatoid arthritis and hearing disorders, Acta Med. Iran. 48 (2010) 371–373.
[32] A. Emamifar, I.M.J. Hansen, An update on hearing impairment in patients with rheumatoid arthritis, J. Otolaryngol. 13 (2018) 1–4.
[33] A. Ogata, T. Hirano, Y. Hishitani, T. Tanaka, Safety and efficacy of tocilizumab for the treatment of rheumatoid arthritis, Clin Med Insights Arthritis Musculoskelet Disord 5 (2012) 27–42.
[34] T. Tanaka, Y. Hishitani, A. Ogata, Monoclonal antibodies in rheumatoid arthritis: comparative effectiveness of tocilizumab with tumor necrosis factor inhibitors, Biologics 8 (2014) 141–153.
[35] A. Ogata, T. Morita, Y. Yoshida, T. Tanaka, Subcutaneous formulation of tocilizumab for treatment of rheumatoid arthritis, Ther. Deliv. 6 (2015) 283–295.
[36] T.J. Yoo, K. Tomoda, A.D. Hernandez, Type II collagen-induced autoimmune inner ear lesions in guinea pigs, Ann. Otol. Rhinol. Laryngol. Suppl. 113 (1984) 3–5.
[37] T.J. Yoo, J.M. Stuart, A.H. Kang, A.S. Townes, K. Tomoda, S. Dixit, Type II collagen autoimmunity in otosclerosis and Meniere's disease, Science 217 (1982) 1153–1155.
[38] R.J. Goodyear, G.P. Richardson, Extracellular matrices associated with the apical surfaces of sensory epithelia in the inner ear: molecular and structural diversity, J. Neurobiol. 53 (2002) 212–227.
[39] N.B. Slepecky, J.E. Savage, T.J. Yoo, Localization of type II, IX and V collagen in the inner ear, Acta Otolaryngol. 112 (1992) 611–617.
[40] Z.F. Mann, W. Chang, K.Y. Lee, K.A. King, M.W. Kelley, Expression and function of scleraxis in the developing auditory system, PLoS One 8 (2013) e75521.
[41] A.J. Hudspeth, How the ear's works work, Nature 341 (1989) 397–404.
[42] A. Flock, Transducing mechanisms in the lateral line canal organ receptors, Cold Spring Harb. Symp. Quant. Biol. 30 (1965) 133–145.
[43] K. Okuyama, T. Kawaguchi, Molecular and fibrillar structures of collagen, Kobunshi Ronbunshu 67 (2010) 229–247.
[44] T. Harada, T. Matsunaga, K. Hong, K. Inoue, Endolymphatic hydrops and III type allergic reaction, Acta Otolaryngol. 97 (1984) 450–459.
[45] B. Gloddek, A.F. Ryan, J.P. Harris, Homing of lymphocytes to the inner ear, Acta Otolaryngol. 111 (1991) 1051–1059.
[46] J.P. Harris, A.F. Ryan, Fundamental immune mechanisms of the brain and inner ear, Otolaryngol. Head Neck Surg. 112 (1995) 639–653.
[47] C.A. Solares, A.E. Edling, J.M. Johnson, M.J. Baek, K. Hirose, G.B. Hughes, et al., Murine autoimmune hearing loss mediated by CD4+ T cells specific for inner ear peptides, J. Clin. Invest. 113 (2004) 1210–1217.
[48] F. Salvinelli, F. Cancilleri, M. Casale, V. Luccarelli, V. Di Peco, L. D'Ascanio, et al., Hearing thresholds in patients affected by rheumatoid arthritis, Clin. Otolaryngol. Allied Sci. 29 (2004) 75–79.
[49] T. Imai, A. Uno, T. Kitahara, T. Okumura, A. Horii, Y. Ohta, et al., Evaluation of endolymphatic hydrops using 3-T MRI after intravenous gadolinium injection, Eur. Arch. Otorrinolaringol. 274 (2017) 4103–4111.
[50] E. Degerman, R. In't Zandt, A. Palbrink, M. Magnusson, Endolymphatic hydrops induced by different mechanisms responds differentially to spironolactone: a rationale for understanding the diversity of treatment responses in hydropic inner ear disease, Acta Otolaryngol. 139 (2019) 685–691.
[51] P. Wangemann, Comparison of ion transport mechanisms between vestibular dark cells and strial marginal cells, Hear. Res. 90 (1995) 149–157.
[52] J.D. Johns, S.M. Adadey, M. Hoa, The role of the stria vascularis in neglected otologic disease, Hear. Res. 428 (2023) 108682.
[53] L. Frejo, A. Gallego-Martinez, T. Requena, E. Martin-Sanz, J.C. Amor-Dorado, A. Soto-Varela, et al., Proinflammatory cytokines and response to molds in mononuclear cells of patients with Meniere disease, Sci. Rep. 8 (2018) 5974.
[54] S. Shah, S. Chidarala, S. Jeong, K. Zhang, S.A. Nguyen, R. Wilkinson, et al., Secondary autoimmune immune ear disease (AIED): a systematic review and meta-analysis on vestibular manifestations of systemic autoimmune and inflammatory disorders, Clin. Rheumatol. 42 (2023) 2747–2759.